Evolutionary Ecology
https://doi.org/10.1007/s10682-022-10206-4

ORIGINAL PAPER

Across the Gobi Desert: impact of landscape features on the biogeography and phylogeographically-structured release calls of the Mongolian Toad, *Strauchbufo raddei* in East Asia

Siti N. Othman[1] · Minjee Choe[2] · Ming-Feng Chuang[3] · Zoljargal Purevdorj[4] · Irina Maslova[5] · Natalya Alekseevna Schepina[6] · Yikweon Jang[2] · Amaël Borzée[1]

Received: 30 March 2022 / Accepted: 12 July 2022

Abstract
Landscape structures drive biogeographic patterns and population connectivity of animals distributed across diverse biotopes. Here, we provide a fresh insight on the impact of five landscape types in East Asia on the phylogeography and acoustic variability of the widespread Mongolian Toad, *Strauchbufo raddei*. For the first time, we reconstructed the biogeography of *S. raddei* over the species' entire range throughout East Asia ($N = 293$; assembled up to 2,613 bp of concatenated *CR-COI*-12S rRNA-16S rRNA) using fossil-based molecular dating and genetic connectivity assessments. In addition, we addressed past population dynamics in relation to landscape types, and geographic variations in release calls for the clades occurring in the steppes of northern Mongolia and the Amur River basin ($N = 147$). Our results recovered two separate ancestors of *S. raddei* in East Asia, supporting a basal split between the northeastern and southern lineages in the Middle Miocene, c. 9.48–13.77 Mya. Ancestral range estimates suggested a Late Miocene radiation within the northeastern lineage, likely due to aridity-induced vicariance and dispersal from the central Asian steppes, c. 7.89 (5.25–11.50) Mya. The southern lineage emerged subsequently from glacial refugia, c. 6.84 (3.48–2.63) Mya, expanding northward and crossing the Gobi Desert and current-day Mongolia, c. 2.60 (1.15–3.72) Mya. At the exception of the pre-Tibetan Plateau clade, our reconstruction of migration trajectories highlighted the presence of effective gene flow across other landscapes, notably among the central and northeastern Chinese clades in the habitats defined as steppe, river basin and canyon. Significant variation in release calls between the clades in northern Mongolia and the Amur River Basin reflected the isolation between the two clades, and supported the presence of a northern refugium and post-glacial expansion of the southern lineage into northwestern Mongolia. In contrast with prior studies, our finding indicates that release calls can reflect phylogeographic patterns.

Siti N. Othman and Minjee Choe have authors equally contributed on this article.

Extended author information available on the last page of the article

Published online: 27 August 2022

Keywords Release calls · Geographic variation · Gobi · Migration · Barriers · Glacial refugia

Background

Landscape features drive ecological dynamics, which in turn contribute to environmental variations (Goigel and Turner 1989). As a result, the variability in environmental conditions impacts biogeography (Kent 2007), genetic and biological diversity (Andren 1994; Adams et al. 2016), and selection and evolution (Barton and Turelli 1987). In particular, the diversity of landscapes and environmental factors regulate the movement and gene flow of taxa (Okamiya and Kusano 2019), affecting the size of home ranges (Katayama et al. 2014) and influencing resource availability (Wang et al. 2012). Hence, understanding the biogeography of model taxa distributed over vast landscapes helps address complex issues such as the patterns of colonisation across landscape corridors (Bartelt and Klaver 2017), behavioural adaptation, and evolution of phenotypic traits in changing landscapes (Joly 2019).

The landscape of the Eastern Palearctic is characterised by a continuous landmass, with variable landscapes that have shaped the eco-phylogeography of species in the region. The Eastern Palearctic includes and connects several major biomes, being bordered by the Qinghai Tibetan Plateau (QTP), which originated from the orogenesis of adjacent mountains in southwestern China (Xing and Ree 2017). The QTP is channelling large river basins and reservoirs, especially in northern and northeastern Asia (Liu et al. 2020). The orogenesis of the QTP also induced the desertification of central Asia, and the development of steppe-desert biomes such as the Gobi Desert (Lu et al. 2019), further delineating the boundaries of the Eastern Palearctic.

The understanding of landscape dynamics needed to interpret biogeographic patterns across landscapes is however insufficient in East Asian (Favre et al. 2015). Specifically for anurans, as landscape connectivity is key for dispersal (Igawa et al. 2013) but also a source of substantial variations in breeding habitats (Li et al. 2020), abiotic factors (Mott 2010), genetic structure (Homola et al. 2019) and population abundance (Knutson et al. 1999). Interestingly, the Mongolian Toad, *Strauchbufo raddei* Strauch, 1876 inhabits diverse biotopes (Litvinchuk et al. 2020), including deserts and grasslands in Eastern Siberia, Mongolia and western China, and river basins in northeastern China, the northern Korean Peninsula (Borzée et al. 2021b) and the Amur Basin in Russia (Kuzmin and Ischenko 1997). Similarly, the species occurs across a wide range of elevations, reaching as high as 3000 m in the western Chinese mountains close to the QTP (Kuzmin et al. 2004). These wide latitudinal and longitudinal ranges support the use of *S. raddei* as a model system to relate genetic connectivity and landscapes-level phylogeography (see maps in Figs. 1, 2and3).

The biogeographic origin of *S. raddei* in East Asia is unclear. At the time of writing, most of the phylogeographic investigations revolve around the Chinese clades of *S. raddei*, defined into two separated western and an eastern mitochondrial lineages (Dong et al. 2012). Despite the recovery of these two lineages in China, the pattern of emergence of *S. raddei* and subsequent continental radiations in East Asia are still unresolved (Malakhov 2004). Nevertheless, recent clarifications regarding the distribution of *S. raddei* fossils, based on past habitat suitability models (Litvinchuk et al. 2020), provided much needed estimates for molecular dating using fossil calibrations. The use of fossil evidences as a primary calibration, combined with dating estimates of earlier works (Stöck et al. 2006;

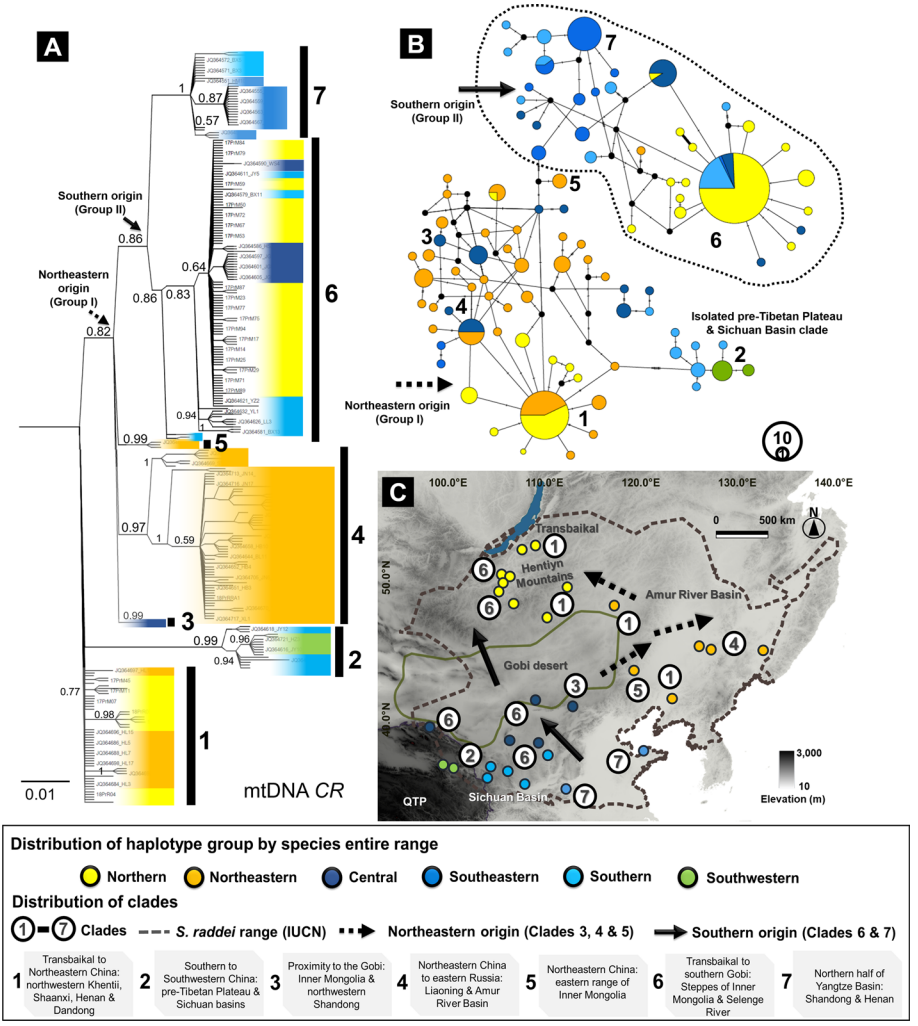

Fig. 1 Haplotype network and phylogenetic relationship among East Asian *Strauchbufo raddei.* **a** Bayesian Inference (BI) tree of East Asian *S. raddei* inferred from an 838 bp-long mtDNA *CR* fragment from 293 individuals. The node values indicate the Bayesian posterior probability (BPP) of each clade. The BI tree recovered seven monophyletic groups (Clades 1–7) for *S. raddei* across its range. The clades clustered into two divergent lineages. **b** Haplotype network derived from the same mtDNA *CR* dataset using a Median Joining (MJ) analysis. The colour codes used for each haplotype group are matching with the colour used in the BI tree, and their distribution on the map. **c** Geographic distribution of clades across the entire range of *S. raddei* in East Asia. The symbols, colour of sampling site and the geographic regions related to the map are described in the legend

Dong et al. 2012; Borzée et al. 2017; Othman et al. 2020) and large samples sizes across the totality of the species' range helps reveal the patterns of phylogeography and landscape connectivity through time.

Hypothetically, the Pleistocene glacial oscillations have affected the genetic structure and patterns of continental radiations of Asian bufonids (Garcia-Porta et al. 2012; Othman

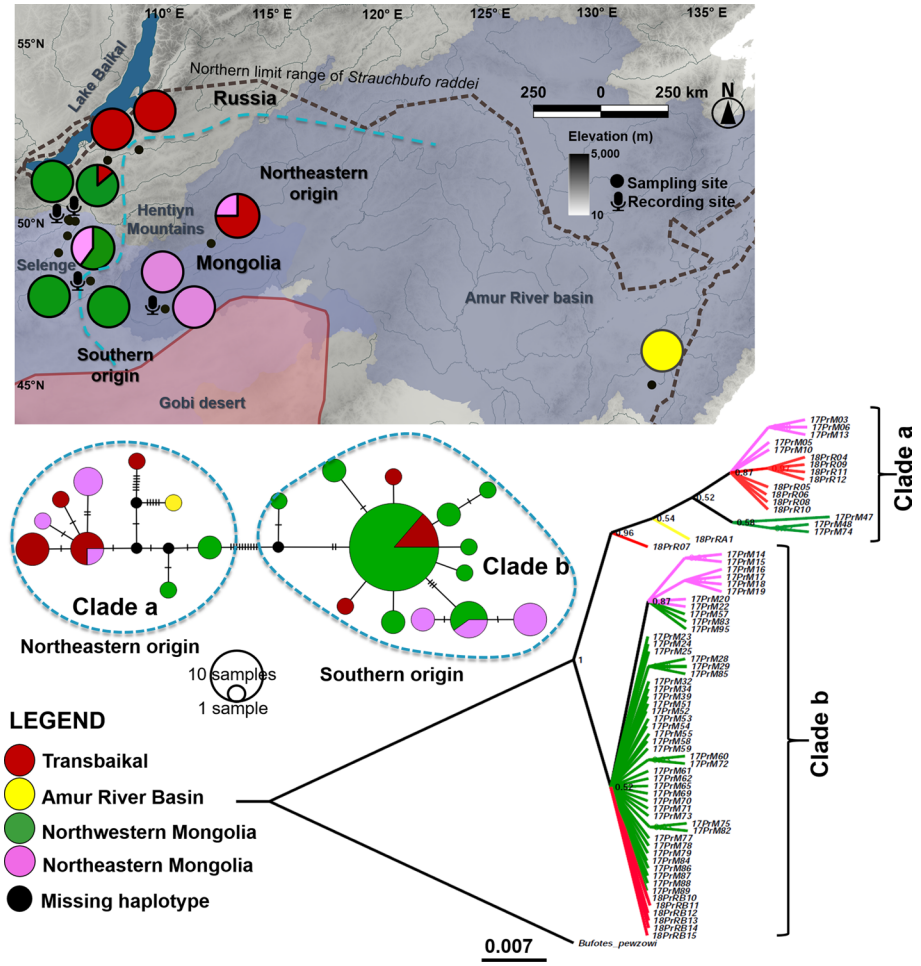

Fig. 2 Bayesian Inference (BI) tree and median joining network of two divergent northern clades of *Strauchbufo raddei* in northeast Asia. Analyses based on the concatenated *CR*-12S rRNA-*COI* fragments (1,882 bp) for 70 individuals sampled in north and northwestern Mongolia, southeastern Baikal and Amur River Basin. The numbers at the nodes indicate the values for posterior probability (PP) with *Bufotes pewzowi* as outgroup. The scale bar represents the nucleotide substitutions rate per site. The colour on the haplotypes network, map and legend are matching, and missing haplotypes are indicated by solid black circles

et al. 2020). The unfavourable conditions during ice ages are likely to have wiped out western Palearctic *S. raddei* (Malakhov 2004; Ratnikov 2016), while the modern Asian lineage of the species has survived the landscape-mitigated effects of glaciations by shifting range towards Eastern Palearctic refugia (Malakhov 2004; Litvinchuk et al. 2020). This hypothesis is coherent with the biogeography of closely related toad species, as the climatic changes and sea level fluctuations during ice-ages have driven the phylogeography of *Bufo* sp. distributed in northeastern Asia, including for instance *B. gargarizans* (Borzée et al. 2017), *B. sachalinensis sachalinensis* (Othman et al. 2022) and *B. stejnegeri* (Fong et al. 2020). Despite the minimal impact of glaciations on Chinese *S. raddei* in the southern

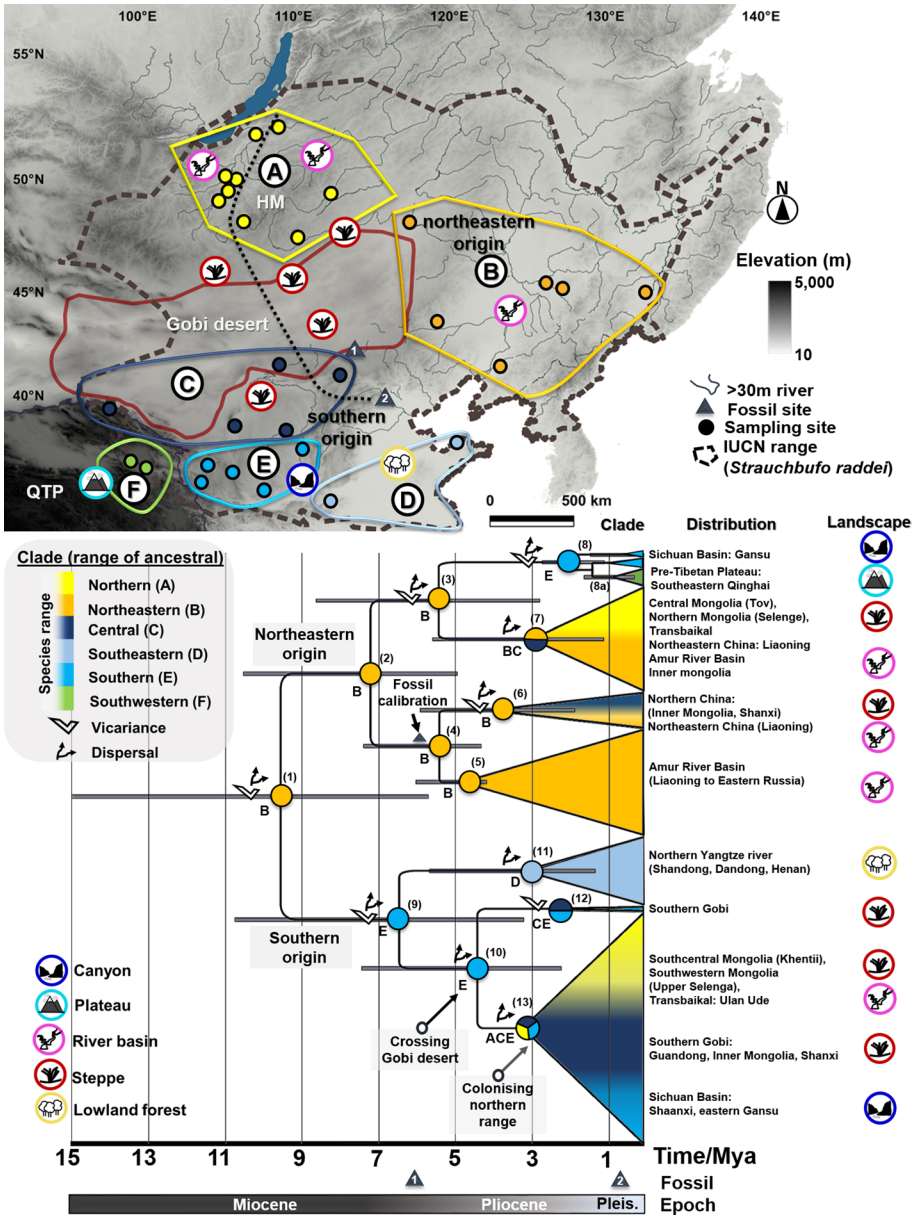

Fig. 3 Calibrated tree with estimated divergence for *Strauchbufo raddei* ($N=288$) inferred from 893 bp of the *CR* fragment. The colour for the clades and the origins of ranges are similarly colour coded. The numbering of each node in bracket matches the node reference number in Table 1. The specific landscape for each clade ($N=6$) is embedded next to the corresponding node of the timetree. QTP stands for Qinghai Tibetan Plateau and HM for Hentiyn Mountains

part of the species' range (Dong et al. 2012), the presence of glacial-driven refugia in Asia needs to be confirmed through a population dynamic lens, focusing on the northwestern limit of the current range of *S. raddei*.

In addition to phylogenetic analyses, acoustic characters are useful to infer geographic variations (Jang et al. 2011) and to retrace divergence in relation to habitat selections (Ryan et al. 1990; Pröhl et al. 2010). To a certain extent, acoustic signals have contributed to the evaluation of taxonomic relationships (Forti et al. 2017). However, most bioacoustic studies are focused on advertisement calls in anuran species (Köhler et al. 2017), even though most species can produce several types of calls (Chuang et al. 2016), such as release, contact or distress calls (Price and Meyer 1979). The release call, a type of a call emitted by an individual when its dorsum, flanks, or axillary region are in contact with another male attempting to amplex (White et al. 2017; Stănescu et al. 2019), is an important acoustic trait for sexual recognition in toad (Price and Meyer 1979). For species that highly rely on acoustic signals, variations in these signals are expected (Lee et al. 2016). Specifically for *S. raddei*, release calls may reflect historical factors linked to phylogeographic structures, and may provide additional support to the genetic relations among populations (Kuzmin and Ischenko 1997). In the northern regions of *S. raddei* distribution, the Hentiyn mountain range physically segregates northwestern and northeastern Mongolia (White et al. 2017), a pattern possibly matching with the phylogeographic structure and patterns of divergence in call properties.

Here, the goals of our study are: (1) to infer the biogeographic pattern of *S. raddei* across the totality of its range in East Asia using fossil-based calibration for molecular dating, (2) to clarify the effect of variability in landscape features on the pattern of distribution and genetic structure of *S. raddei* in East Asia and, (3) to characterise the impact of glacial refugia and landscape fragmentation on phenotypic variations, here the release calls between two segregated Mongolian clades.

Methods

Species, study region and molecular sampling

Strauchbufo raddei is not listed as a threatened species, and it is one of the most widespread species in northeast Asia according to the International Union for Conservation of Nature (IUCN) Red List of Threatened Species (Kuzmin et al. 2004). As the study was conducted, the northern clade of *S. raddei* was under sampled and no sequences were available in online databases, so we collected samples from 10 sites in northern Mongolia and southeastern Russia (N individual = 146; Table S1; see maps in Figs. 1 and 2). The sampling localities in Mongolia (N sample = 127; N site = 7) ranged from the northwestern border (lower and upper Selenge River) to central Mongolia (Khentii, Dornod and Tov, Table S1, Fig. 1). Samples in Russia covered the southwestern (Baikal Lake) and eastern (Amur River Basin) regions (N sample = 19, N site = 3; Table S1, Fig. 1).

Release calls sampling

Although the validity of release call trait as a natural evolutionary signal is still debated (Reichert and Höbel 2018; Stănescu et al. 2019), a recent study on anurans demonstrated that release calls are phylogenetically informative and can be used for species identification (Mângia et al. 2019). To clarify the impact of landscape barriers and the potential reproductive isolation, we tested if the release calls of two separate populations of northern *S. raddei* were different. The populations where the calls were recorded were geographically

segregated by a physical barrier, the Hentiyn Mountains (Fig. 2). All individuals were recorded in wetlands, and we classified each site into lake, oxbow or pond based on vegetation level, adapted from the limnologic definition of water bodies (Biggs et al. 2005).

We first captured all individuals by hand with plastic bags to avoid physical contact and avoid potential disease transmission and maintained an individual identification for buccal swabs and recording. We then identified the sex of each individual by checking the presence of nuptial pads. Finally, we recorded the release calls of all males by gently touching their back or flanks (Castellano et al. 2002), holding the individuals by their hind legs but with their body resting on a substrate to prevent biases in recordings introduced by holding the individuals and physically modifying call structure, or modifying call properties by warming the body of the toad through contact. Each toad was handled for less than two minutes (n individuals = 35; n calls matched with molecular samples = 29; Table S2). All calls were recorded in situ with a digital recorder (TASCAM DR-40; Montebello, CA, USA) coupled with a shotgun microphone (HTDZ HT-81; China).

During the recording, each male was held 10–20 cm away from the microphone, to ensure proper quality, while avoiding saturation. We relied on a minimum of five consecutive calls from each individual and we analysed the calls using Raven Pro v1.5 (Cornell Lab of Ornithology, Ithaca, NY) to extract acoustic features. Frequencies higher than 15 kHz were filtered out to remove unnecessary background noise. The aural components extracted were call period, call duration, rise time, fall time, and dominant frequency (Fig. S1).

To control the effect of body size and temperature on the parameters of call properties, we measured the snout-vent length (SVL) of each individual to the nearest 0.01 mm using a digital calliper (Insize, GA, USA) and the weight to the nearest 0.01 g using a digital scale (MH-500, China). We also recorded the ambient temperatures using a digital thermometer (Amazon, HDE, USA). The data for calls properties, environmental temperature, SVL and length are in Table S2.

Laboratory protocols

We kept the collected swabs with desiccants immediately after collection to prevent DNA degradation, up until proper storage at − 20 °C before DNA extraction. We then extracted the genomic DNA from the buccal swabs using the DNeasy Blood and Tissue Extraction Kit (Qiagen, Group, Hilden, Germany). The concentration of each DNA sample was determined using a NanoDrop™ 2000/2000c and a spectrophotometer (ThermoFisher Scientific). We then amplified the four mtDNA gene fragments with a Polymerase Chain Reaction (PCR). First, we amplified the partial 16S rRNA gene fragment using the universal primers adapted from the literature (Kocher et al., 1989; Palumbi, 1996; Fu, 1999; Liu et al., 2000; Table S2). Then, we designed primers pairs for the three other gene fragments, 12S rRNA, the Control Region (*CR*), and the protein-coding *c*-oxidase subunit I (*COI*) based on homologous sequences from Genbank (Table S2).

For each primer pair, we prepared PCR reactions in a total volume of 20 µl per tube. The PCR reagents contained a final concentration of 0.125 µM for each forward and reverse primer, 0.2 mM of dNTPs mix (Takara; Shiga, Japan), 1.875 mM of magnesium chloride ($MgCl_2$), 1 × Ex taq Buffer (Takara; Shiga, Japan) and 0.1 unit/µL of Ex taq (HR001A, Takara; Shiga, Japan). For each PCR reaction, we added the DNA template with a concentration of 30–50 ng/µL and double distilled water to make up the final volume for the reaction. We then conducted the PCR amplifications on a SimpliAmp Thermal Cycler (Applied

Biosystem, USA) with the following protocol: pre-denaturation for 5 min at 95 °C, 35 cycles of denaturation at 95 °C for 1 min, annealing at 50–55 °C for 30 s (annealing temperature of each primer pair in Table S3), elongation at 72 °C for 1 min and a final elongation at 72 °C for 10 min.

We ran the final PCR products on 1.5% agarose gels in 1X TBE buffer for electrophoresis to verify if the gene fragments were amplified correctly. We then purified our samples with rAP (rAPid Alkaline Phosphatase with Exonuclease 1), using 10 µl of PCR products and 4 µl of rAP mixture. Sequencing was carried out with the BigDye™ Terminator v3.1 Cycle Sequencing Kit (Thermo Fisher Scientific; Gangnam, Republic of Korea) in an Applied Biosystems DNA Analyzer (3730/3730xl, Thermo Fisher Scientific; Gangnam, Korea) by Cosmo Genetech Corp. (Seoul, Republic of Korea). Sequencing was conducted in both forward and reverse directions, and we deposited all sequences generated in this study in Genbank (see accession number in Table S1).

Designation of datasets

We prepared two types of datasets to answer different questions, one focusing on clades in East Asia in general and the other restricted to the northern clades of *S. raddei*. The two objectives were: (i) resolving the phylogenetic relationship, population structure, molecular dating and ancestral range of *S. raddei* across the totality of its range. To do so, we created a dataset of East Asian *S. raddei*, including a total of 293 mtDNA *CR* sequences (893 bp), combining our Mongolian and Russian samples ($N=108$) with Genbank sequences ($N=185$) retrieved from the literature (Dong et al. 2012) and originating from China. (ii) Resolving the phylogeny, past population dynamic and pattern of release calls within the northern clades of *S. raddei*. For this question, we relied on two datasets, one comprising 2,226 bp from the concatenated *CR*-12S rRNA-16S rRNA-*COI* fragments ($N=53$) and the other comprising 1,882 bp from the concatenated *CR*-12S rRNA-*COI* fragments ($N=72$), including samples from the northern clades ranging from Mongolia to Russia.

Phylogenetics and haplotype network analyses

We analysed and trimmed all sequences for accuracy with Geneious v.11.0.4 (Kearse et al. 2012). We assembled and aligned the sequences for each gene fragment using Clustal W v.2.0 (Larkin et al. 2007). The final lengths of each gene fragment were 369 bp for 12S rRNA, 473 bp for 16S rRNA, 893 bp for *CR*, and 491 bp for *CO1*.

We computed the unique haplotype number and haplotype diversity (H) for the East Asian and the northern clades datasets using DnaSP v5.10.1 (Librado and Rozas 2009). Here, we distributed the haplotypes from the *CR* fragment for all of East Asia into six groups based on geographic information. The groups were (Fig. 1): (i) northern range—Mongolia and Transbaikal ($N=105$), (ii) northeastern range—Amur River Basin ($N=69$), (iii) central range—steppes of the Gobi Desert ($N=38$), (iv) southeastern range—northern Yangtze ($N=35$), (v) southern range—Sichuan Basin ($N=38$), and (vi) southwestern range—pre-Tibetan Plateau ($N=8$). We then computed the median-joining haplotype network using PopART v.1.7 (Leigh and Bryant 2015). We repeated the analysis on the dataset restricted to the northern clades for the concatenated *CR-12S-COI* fragments ($N=70$ after trimming). The haplotype groups were assigned to four geographic regions (Fig. 2): (i) Transbaikal ($N=15$), (ii) Amur River Basin ($N=1$), (iii) northwestern Mongolia ($N=41$), and (iv) northcentral Mongolia ($N=13$).

To determine whether the populations experienced a spatial range expansion, constriction, or stationary population history (Tajima 1989), we calculated the mismatch distribution and tested the neutrality of the *CR* fragment with Tajima's D (Tajima 1989) and Fu's Fs (Fu 1997) for the East Asian dataset (see details in Table S4).

To resolve the phylogenetic relationships within *S. raddei*, we determined the best sequence substitution model for each gene fragment with the Bayesian Information Criteria (BIC) algorithm using Partition Finder v.2.0 (Lanfear et al. 2017). In all four mtDNA fragments, we recovered six partitions based on a fixed position for non–coding fragments and the three codon positions rule for protein coding fragments (Table S5). We then reconstructed a Bayesian Inference (BI) tree based on the *CR* fragment for the East Asian dataset and the concatenated *CR*-12S rRNA-*COI* fragments for the northern clades dataset using Mrbayes v.3.1.2 (Ronquist et al. 2012). We included the Eurasian bufonid species *Bufotes pewzowi* as an outgroup for each dataset. We ran the analyses for 50 million generations of Markov Chain Monte Carlo (MCMC) with four independent chains. We sampled every 1000th tree from the total trees generated and let the analysis run until the trees reached convergence (split frequencies value lower than 0.05). Finally, we visualized the trees using FigTree v.1.3.1 (Rambaut et al. 2018).

Fossil-based molecular dating and ancestral range reconstruction

Our goals were to address two phylogeographic questions; (i) the pattern of emergence of modern Asian *S. raddei* in the Eastern Palearctic, and (ii) the pattern of continental radiations within the clades recovered in East Asia. Here we resolved the phylogeographic patterns of *S. raddei* across the totality of its range in East Asia. To do so, we dated the phylogenetic tree inferred from the *CR* fragment originating from the East Asian dataset ($N = 288$ after trimming).

We first specified the best substitution model for the *CR* fragment using the bModelTest package (Bouckaert and Drummond 2017). We obtained SYM/GTR as the best ranked evolutionary model for our dataset with the highest posterior support of 0.50% and a cumulative support of 100%.

We then set three calibration points in our molecular dating estimates, established from the combination of both fossils and palaeogeological events as the primary source of dating calibrations. Additionally, we added secondary calibrations obtained from previous estimates based on the divergence time for the Chinese clades (Dong et al. 2012). Due to the lack of clarity in the type and distribution of fossil of *S. raddei*, we selected only relevant fossils (Böhme and Ilg 2003; Table S6), distributed within the present and past range of the species, as proposed by Litvinchuk et al. (2020). The fossil selected as calibration points were: (i) the Messinian-Zanclean fossil of East Asian *Bufotes raddei* recorded in the Zhoukoudian locality in Inner Mongolia, China (7.1–5.3 Mya; Roček et al. 2011), (ii) the Pleistocene fossil of *B. raddei* from Beijing, China (0.126–0.78 Mya; Ratnikov 2001), (iii) the isolation of the south western Chinese clade distributed east of the QTP (0.25–0.002 Mya; Dong et al. 2012), and (iv) the Qinzang movement event estimated during the Quaternary as this phase has already been linked with the emergence of other anuran clades with similar ranges (e.g. *Babina pleuraden*; c. 2.5–1.8 Mya; Li et al. 2012).

In order to increase number of ingroup taxa and the variability in sampling locations, we unified our dataset containing sequences isolated from Mongolian and Russian *S. raddei* with sequences from clades distributed in China and retrieved from Dong et al. (2012). Thus, using a single *CR* fragment is appropriate for a first approach to the biogeography of

S. raddei across its entire distribution. We estimated the divergence time with the *CR* fragment using a mixed method including relaxed and strict molecular clock models, with fixed and non-fixed rates of divergence for *CR*, based on the molecular dating methods proposed by Bletsa et al. (2019), and recommended by Othman et al. (2022) for Asian toads. For the relaxed clock, we did not specify any clock rate. Following the assumption that the fossil age is within its minimal range and to avoid any overestimation, we enforced a lognormal distribution prior to the fossil-based calibration and a normal distribution prior on the paleogeological events and secondary calibrations. For the strict clock, we fixed the prior to the clock rate of 7.3×10^{-9}, based on a divergence rate of 1.278%/Mya for the mtDNA *CR* of the *Bufotes viridis* subgroup, estimated by Stöck et al. (2006). The estimate is based a geological event as the main source of calibration: the formation of the Strait of Sicily disconnecting North Africa and Sicily (c. 5.3–5.0 Mya) and resulting in the separation between the northern and southern *B. viridis* groups.

We ran a few simulations prior to the analyses to test the most appropriate tree priors. We selected the birth–death and coalescent constant models as the best tree priors for relaxed and strict clock methods, respectively. We computed the calibrated trees with BEAST v.2.6.1 (Bouckaert et al. 2019) using two independent runs of ten million MCMC chains. The convergence of the tree was diagnosed with Tracer v.1.7 (Rambaut et al. 2018), and we generated a Maximum Clade Credibility (MCC) tree by discarding 20% of the trees with a probability below 0.5 using Tree Annotator (Bouckaert et al. 2019) implemented in the BEAST environment.

We further reconstructed the ancestral distribution of *S. raddei* in East Asia based on the dated *CR* tree using a Bayesian approach in RASP v.4.0 (Yu et al. 2015). Here, we designated eight possible ancestral ranges (named from A to H; Fig. 3) based on the geographic regions of the clades across the totality of *S. raddei* range. We assigned each node of the time tree to its specific range, with the predefined ancestral range such as; (A) northern range; covering northwestern Mongolia to the Transbaikal region, (B) northeastern range; covering northern China to the Amur River Basin in Russia, (C) central range; covering the steppes of the Gobi, (D) southeastern range; covering the northern half of Yangtze river basin, (E) southern range; covering the Sichuan basin, and (F) southwestern range; covering the pre-Tibetan Plateau. We then analysed the data for each biogeographic region through a statistical dispersal-extinction-cladogenesis (S-DEC) analysis. Here, we inserted the coordinates of each estimated ancestral range (A–F) as our input data in the S-DEC parameters setup, and included the locations of the oldest fossil to calculate the probability of ancestral range for each ancestral clade. To obtain the most probable area as the range of ancestry for each recovered clade, we computed a Bayesian inference analysis for discrete areas (BAYarea; Landis et al. 2013) on the condensed time trees, with 10 million MCMC generations and a burn in of 500,000 generations.

Landscape, genetic connectivity and gene flow

To assess the influence of geographic factors on the genetic variation, we ran a mantel test between genetic (F_{ST}) and geographic distances (km) among the five groups defined earlier with ARLEQUIN v.3.5.1.3 (Excoffier and Lischer 2010) using 100,000 permutations. We visualised the correlation between the two matrices with ORIGIN v.9.0 (Seifert 2014). The geographic distance was determined as the shortest distance between every two localities and was calculated in Google Earth Pro v.7.3 (Google Inc., Mountain View, CA). We converted the coordinates of the populations of interest into virtual points as represented

by the Voronoi triangulation (Manni et al. 2004). We extracted the distance matrices from multiple nucleotides substitution models of evolution: Jukes-cantor (JC; Jukes and Cantor 1969), Maximum likelihood composite (Varin et al. 2011), Tamura-Nei (Tamura and Nei 1993), Kimura-2-Parameter (K2P; Kimura 1980), F_{ST} and p-distance in the form of 100 bootstraps of matrices.

To determine the efficiency of landscape features (i.e. Hentiyn Mountains and Gobi desert) as barriers among the four populations of *S. raddei* distributed in northern-most range (Mongolia and Transbaikal) and the ten populations distributed across the entire distribution, we calculated the possible genetic barriers using the Monmonier algorithm (Monmonier 1989). Here, we generated 100 bootstraps in the form of Slatkin's matrices for both northern range and species entire range datasets. Finally, we computed the analyses for genetic barriers using the simulation of the Voronoi diagram in Barrier v.2.2 (Manni et al. 2004). Here, we computed the migration trajectories and gene flow rate for a total of 165 *CR* fragments (1,201 bp) of *S. raddei* across East Asia. We designated the populations based on five landscape-specific clades that we categorised into: (i) Desert-grassland (*n* gene copies = 37) representing the clades inhabiting the central Asia deserts, the steppe of north central Mongolia and northern China; (ii) Lowland-forest ($N = 27$)—representing the clades distributed on the northern half of the Yangtze Basin; (iii) Canyon ($N = 39$)—representing the clades inhabiting mountain ranges (> 1000 m) surrounding the Sichuan Basin; (iv) Plateau ($N = 18$)—representing the clades distributed at the high elevation (> 3000 m) of the eastern QTP in southwestern part of the range; and (v) River basins ($N = 44$) representing the clades distributed in the Mongolian river basins, and northeastern Asia. Using a Bayesian coalescent approach implemented in MIGRATE-n v.4.4.3 (Beerli et al. 2019), we estimated the rate of mutation-scaled migration (M) under the assumption that populations are not in the state of migration-drift equilibrium and not under the Hardy–Weinberg Law (Li et al. 2017). In our analysis, we assumed the mutation rates of the mtDNA *CR* to be heterogeneous among sites using a Hidden Markov Model with the F84 mutation model. Our analyses included four long chains with 10 million generations MCMC chains. We replicated the analyses three times and summed the means obtained for Θ. We ran the computation with three long chains and repeated the analyses for four replicates. We calculated the effective number of migrants using the relation ($N\,m = \Theta \times M/2$, where Θ is the mutation-scaled effective population size) to enable a comparison with contemporary estimates.

Past population dynamics of northern clades

We then tested the hypothesis of range shifts in *S. raddei* from the western and central Palearctic to the eastern Palearctic during glaciations (Malakhov 2004). The population dynamic focusing on the Chinese clades demonstrated a weak impact of glaciations on the populations, with a potential northern and western glacial refugia (Dong et al. 2012). Here, we further examined the impact of glaciations on *S. raddei* across East Asia by focusing on the pattern of past population dynamic of the two divergent northern clades identified by the phylogeny analyses: the northwestern Mongolian clade originating from the southern edge of the range (Clade A) and the north central Mongolian clade originating from the northeastern part of the range (Clade B). The northern Mongolia-southern Baikal Lake clade is also within the western most limit of *S. raddei*, and so allowed us to test the range shift hypothesis proposed by previous studies. Here, we particularly focused on three phases of glaciations since the last ice age period, following the palaeoecological timeframe proposed by Clark et al. (2009). The three phases of glaciation were: (i) prior

glacial: Last Glacial (c. 50 Kya) to Last Glacial Maximum (LGM; c. 22 Kya), (ii) peak glacial: LGM (c. 22 Kya) to end of glacial period (c.14.5 Kya), and (iii) postglacial period (c.14.5 Kya) to present day.

We ran a Bayesian Coalescent Skyline Plot (BCSP; Drummond et al., 2005) to determine past variations in effective population size inferred from the 1,513 bp of concatenated *CR-COI* fragments obtained from 82 individuals from the northern *S. raddei* clades: Clade A ($N=21$) and Clade B ($N=61$). Using a relaxed clock and a lognormal distribution, with the same fixed clock rate (7.3×10^{-9}), we enforced the calibration points used in the molecular dating section and selected the Bayesian Coalescent Constant as prior. We computed the analysis with a 10 million MCMC chains run and repeated the run for each clade twice. We assembled the trees generated using LogCombiner v.2.6.6 (Bouckaert et al. 2019), diagnosed the convergence of the trees and generated the BSCP plots using Tracer v.1.7 (Rambaut et al. 2018), implemented in the BEAST environment.

Statistical analyses for acoustic data

We calculated Spearman's rank correlations between the averages of each call property and ambient temperature (Table S7). We also ran the same test for the averages of each call property and body condition. To acquire a body mass-based measure of body condition for each calling male, we calculated the residuals after regressing the cube root of the mass against the body length for each individual. We expressed these residuals relative to SVL to calculate a condition index to control for the impact of this variable on call properties in downstream analyses. To control for the habitat types (pond, oxbow, and lake) where the calling males were collected, we compared the difference in the release call and body size traits between habitats with a multivariate analysis of variance (MANOVA) followed by a Tukey HSD post hoc test to compare the pairwise differences with SVL as a covariate. The call properties were not adjusted by standardizing the ambient temperature as we found no significant relationship between temperature and release call traits (Table S7). Following the phylogenetic relationship that highlighted two divergent clades with eight males from the northeastern lineage (Clade A) and 18 males from the southern lineage (Clade B), we used a MANOVA to evaluate the variations in release calls between the two clades. All statistical analyses on the release call data were processed using STATA (Stata Corp 2017).

Results

Phylogenetic analyses and haplotype networks

The haplotype network for the *CR* fragment (898 bp; $N=293$; variable sites of sequence = 71) for *Strauchbufo raddei* across its whole range in East Asia resulted in 50 haplotypes, with a diversity of 0.89 in 10 geographic regions distributed across continental northeast Asia (Fig. 1). Haplotypes for the populations in China diverged into two groups, segregated into a northern and a southern group (Fig. 1; Table S3). Haplotypes for the populations in Mongolia followed the same pattern of segregation, matching with a northwestern and a northeastern group (Table S3). Similarly, Russian haplotypes distributed into two different geographic regions, the southeastern Baikal and the Amur River Basin groups (Table S3).

Bayesian inference (BI) from the *CR* fragment increased the resolution of the phylogenetic relationship among *S. raddei* in East Asia, recovering seven clades (referred as Clades 1–7; Fig. 1). Here, the clades were clustered into two groups: northeastern and southern (named as Group I and Group II; Table S4; matching with the dashed and solid arrows on Fig. 1). At the basal node, we partially resolved clade 1, represented by *S. raddei* in the northern and northeastern ranges, i.e. northwestern Khentii, Transbaikal, Shaanxi, Henan and Dandong in Liaoning (Bayesian posterior probability (BPP): 0.77; Fig. 1). Clade 2 recovered *S. raddei* from the southern and southwestern ranges, where the distribution of the species is restricted to the high altitudes (2, 000 to 3,000 m elevation) of the pre-Tibetan Plateau and Sichuan basins (BPP: 0.99; Fig. 1). We also fully resolved Group I, represented by the northeastern lineage and containing three clades (Clades 3, 4, 5; Fig. 1). The three supported clades in Group I included *S. raddei* in its central range, distributed in proximity to the Gobi Desert (Jining and southern Inner Mongolia; Clade 3; BPP = 0.99; Fig. 2), a clade restricted to the northeastern part of the range, occurring from Liaoning in northeastern China and the Amur River Basin in eastern Russia (Clade 4: BPP: 0.97; Fig. 1), and a clade limited to Inner Mongolia in northeastern China (Balinzuoqi, Inner Mongolia; Clade 5; BPP: 0.99; Fig. 1).

The second group represented the southern lineage and included two clades (Group II; Clades 6 and 7; BPP: 0.82: Fig. 1). Group II was a nested clade distributed in the southern, central, and northern range of the species. The nested Clade 6 comprised a subclade in proximity to the southern Gobi Desert: Jiayuguan in Gansu, Helan Mountain in Ningxia and Wula Mountain in Inner Mongolia, and a subclade in northcentral Mongolia covering localities such as Khenti, Dornod, Tov and some individuals from the northern Selenge River Basin (BPP: 0.86; Fig. 1). Finally, Group II also included Clade 7, restricted to the southern and southeastern ranges of the species, i.e. Shandong and Henan (BPP: 1.0; Fig. 1).

We then focused on the haplotype and phylogenetic relationships constructed from the concatenated *CR-12S-COI* fragments in the northern areas of species' range, distributed across Mongolia and Russia. The haplotype network based on the median joining method generated 22 haplotype groups within the four populations in the northern clades, resulting in a haplotype diversity of 0.8170 at 45 variable sites (Fig. 2). Here, the high-resolution tree highlighted two segregated lineages, divided across the western and eastern margins of the Hentiyn Mountains (BPP: 1.0; Clades a and b; Fig. 2). The first clade contained *S. raddei*, predominantly distributed in the northeastern area of the species range (Clade a; BPP: 0.96; Fig. 2). This northeastern clade included a haplotype from the Amur River basin (Lake Khanka) and a haplotype from northcentral Mongolia (Khentii, southeastern margin of the Hentiyn Mountains; Clade a; Fig. 2). The second clade recovered haplotypes ranging from the western margin of the Hentiyn Mountains (Upper and Lower Selenge; Table S1; Fig. 2) and Transbaikal (Ulan-Ude; Table S1; Fig. 2), corresponding with a northern extension of the *S. raddei* clade originating from the southern areas of species' range (Clade b; BPP: 0.56; Fig. 2).

Population structures in northeast Asia

The neutrality tests found a negative Tajima' D in four clades: (i) northwestern Mongolia (Tajima's $D = -0.140$; $p = 0499$; Table S4), (ii) northeastern Asia (Tajima's $D = -0.646$; $p = 0.270$; Table S4), (iii) Sichuan basin (Tajima's $D = -0.862$, $p = 0.202$; Table S4) and pre-Tibetan Plateau (Tajima's $D = -0.933$, $p = 0.260$; Table S4). These

results highlighted an observed frequency of polymorphism lower than expected, and indicated a population size expansion. Additionally, a test for historical population expansion suggested an excess of low-frequency alleles in all populations distributed in East Asia, except in the Amur River Basin population (Fu's Fs: − 1.588, $p = 0.181$; Table S4).

Molecular dating

Overall, our divergence time estimates from both relaxed birth–death and strict coalescent methods were consistent, indicating a small effect of priors. Both methods resulted in trees with similar topologies, at the exception of the sister relationship between the clades from the pre-Tibetan Plateau and central China, which were paraphyletic in the strict coalescent constant tree (Table 1). This, however, did not affect the consistency of other recovered clades, as the placement of crown clade members across stem groups were coherent in both trees.

The dated tree indicated a deep split between the two main clades, with a divergence between the northeastern-and southern-lineages dating from the Middle Miocene c. 13.77–9.48 Mya (Table 1; Fig. 3). The earliest emergence of *S. raddei* in East Asia may have originated from northeastern China, from where this lineage radiated in the Amur River Basin and dispersed over western and northern Mongolia, the Transbaikal regions, and the eastern part of Gobi (Late Miocene; c. 7.14 [HPD 95%: 4.88–10.44]; see relaxed clock estimation in Table 1; Fig. 3). Subsequently, a lineage originating from the southern part of species' range may have emerged (Late Miocene; c. 6.84 [3.48–2.63] Mya; Table 1; Fig. 3), containing the clades currently restricted to the Sichuan basin, northern Yangtze river, southern Gobi and northern Mongolia (Table 1; see southern lineage in Fig. 3).

Within the northeastern lineage, near-simultaneous Pliocene radiations may have given rise to the crown clade in northeastern China (c. 4.84 [8.25–5.70] Mya; Table 1; Fig. 3) and those in close proximity to the eastern Gobi (c. 4.25 [2.02–5.96] Mya; Table 1; Fig. 3). During the Pleistocene, the clade distributed in the Amur River Basin radiated across northcentral Mongolia and the Transbaikal (c. 2.50 [1.20–3.93] Mya; Table 1; Fig. 3). Later, the clade restricted to the pre-Tibetan Plateau may have expanded to the Sichuan basin in the Mid-Pleistocene (c. 1.87 [1.03–2.62] Mya; Table 1; Fig. 3).

The divergence within the southern lineage may have occurred as early as the Lower Pliocene (4.36 [2.10–7.02] Mya; Table 1; Fig. 3), resulting in three crown clades that predominantly inhabiting the Sichuan basin canyons and the steppes of the Gobi. During the mid-Pliocene, vicariance of *S. raddei* in the southern Gobi (i.e. Inner Mongolia and Shaanxi) resulted in the formation of the first crown clade, inhabiting the steppe and canyon landscapes (c.3.55–2.61 Mya; Table 1; Fig. 3).

Concurrently, the second crown clade corresponding to the southern range of *S. raddei,* that distributed in eastern Gansu and Shaanxi, dispersed towards the southern Gobi and colonised the western margin of the Mongolian Plateau and south eastern Baikal c. 2.60 [1.15 – 3.72] Mya (see strict clock estimation; Table 1; Fig. 3). Another dispersal event most likely triggered the formation of the third crown clade that colonised the lowland forest landscape and became restricted to the southeastern area of the species' range (i.e. Henan and Shandong) during the Late Pliocene (c. 0.78 [2.34–0.49] Mya; Table 1; Fig. 3).

Table 1 Reconstruction of ancestral range and molecular dating estimates with strict and relaxed molecular clocks. The mean estimated ages represent the average time between the estimations generated by birth death and coalescent constant priors. The most probably ancestral area is indicated for each clade. The specific numbering of nodes is matching with the nodes in the timetree of Fig. 3

Node number	Lineage origin	Clade (speciation event)	Habitat/landscape type	Relaxed clock with Birth death (median [HPD 95%]/ Mya)	Strict Clock with coalescent (median [HPD 95%]/ Mya)	Mean estimated age (HPD 95%]/ Mya)	Most probably ancestral area using BAYAREA analysis(Ancestral range/ %)	Speciation mode
1	Base of tree	Split between the two lineages: northeastern originated lineage (clades distributed in northern + central + southwestern ranges) versus southern originated lineage (clades distributed in northern + central + Southeastern ranges)	River basin, steppe, canyon, plateau	9.48	13.77	11.63	B–Northeastern range: Amur River Basin (17.60%)	Dispersal and vicariance

Table 1 (continued)

Node number	Lineage origin	Clade (speciation event)	Habitat/landscape type	Relaxed clock with Birth death (median [HPD 95%]/ Mya)	Strict Clock with coalescent (median [HPD 95%]/ Mya)	Mean estimated age (HPD 95%]/ Mya)	Most probably ancestral area using BAYAREA analysis(Ancestral range/ %)	Speciation mode
2	Northeastern	Stem clade of northeastern lineage: comprised of clades originated from the steppes of Gobi and northern Mongolia, Transbaikal, Amur River Basin, and isolated clade of pre-Tibetan Plateau	River basin, mountain range, canyon, steppe	7.14 [4.88−10.44]	10.57	-	B – Northeastern range (24.53%)	Dispersal
4	Northeastern	Stem clade of central and northeastern ranges (covering clades distributed in northwestern Mongolia and Transbaikal)	Steppe and river basin	5.35 [4.25−7.32]	5.77 [4.28−7.49]	5.56 [4.27−7.41]	B- Northeastern range (38.81%)	-

Table 1 (continued)

Node number	Lineage origin	Clade (speciation event)	Habitat/landscape type	Relaxed clock with Birth death (median [HPD 95%]/ Mya)	Strict Clock with coalescent (median [HPD 95%]/ Mya)	Mean estimated age (HPD 95%]/ Mya)	Most probably ancestral area using BAYAREA analysis(Ancestral range/ %)	Speciation mode
3	Northeastern	Stem clade of northern Mongolia, Amur River Basin and pre-Tibetan Plateau	River Basin, Steppe, Canyon, Plateau	5.36 [2.73−8.55]	Not recovered as sister clades, but independent monophyletic clades, respectively	-	B – Northeastern range (23.02%)	Dispersal and vicariance
5	Northeastern	Crown clade restricted to Amur River Basin	River basin	4.76 [4.12−5.19]	4.92 [4.13−6.21]	4.84 [8.25−5.70]	B – Northeastern range: Amur River Basin (24.53%)	-
6	Northeastern	Crown clade of eastern Gobi and Amur River Basin	Steppe and river basin	4.02 [1.81−5.85]	4.47 [2.22−6.06]	4.25 [2.02−5.96]	B – Amur River Basin (38.81%)	Dispersal
7	Northeastern	Crown clade of Amur River Basin (covering northeastern China and Far Eastern Russia)	River basin	2.78 [1.37−4.27]	2.22 [1.02−3.59]	2.50 [1.20−3.93]	B – Amur River Basin (41.64%) BC- Amur River Basin + northern Gobi (40.26%)	Dispersal and vicariance

Table 1 (continued)

Node number	Lineage origin	Clade (speciation event)	Habitat/landscape type	Relaxed clock with Birth death (median [HPD 95%]/ Mya)	Strict Clock with coalescent (median [HPD 95%]/ Mya)	Mean estimated age (HPD 95%]/ Mya)	Most probably ancestral area using BAYAREA analysis(Ancestral range/ %)	Speciation mode
8	Northeastern	Stem clade of northern and central range: northwestern Mongolia + steppes of Gobi + Sichuan canyon	Canyon, steppe and river basin	3.02 [1.43−5.10]	4.15 [2.14−6.79]	3.59 [1.79−5.95]	E – Sichuan Basin (19.53%)	Dispersal
8a	Northeastern	Isolation of pre-Tibetan Plateau clade	Restricted to Plateau area (3,000 m elevation)	1.88 [1.04−2.66]	1.86 [1.02−2.57]	1.87 [1.03−2.62]	E – Sichuan Basin (47.7%) EF Sichuan Basin to pre-Tibetan Plateau (27.31%)	Dispersal
9	Southern	Stem clade of Sichuan Basin, Northern Yangtze river, southern Gobi and southcentral Mongolia	Canyon, river basin, steppe to lowland forest	6.39 [3.14−10.67]	7.28 [3.81−11.96]	6.84 [3.48−2.63]	E – Southern range – Sichuan Basin (15.57%) D –Southeastern range – Northern Yangtze (10.26%)	Dispersal and vicariance
10	Southern	Stem clade of Sichuan Basin, southern part of Gobi, northern Mongolia and Transbaikal	Steppe and canyon	4.36 [2.17−7.36]	4.35 [2.03−6.68]	4.36 [2.10−7.02]	E- Sichuan Basin (19.53%)	-

Table 1 (continued)

Node number	Lineage origin	Clade (speciation event)	Habitat/landscape type	Relaxed clock with Birth death (median [HPD 95%]/ Mya)	Strict Clock with coalescent (median [HPD 95%]/ Mya)	Mean estimated age (HPD 95%]/ Mya)	Most probably ancestral area using BAYAREA analysis(Ancestral range/ %)	Speciation mode
12	Southern	Crown clade of southern Gobi and Sichuan Basin	Steppe and canyon	2.61	3.55	-	CE – Southern Gobi to Sichuan Basin 24.37%)	Vicariance
13	Southern	Stem clade of central-northeastern Asian mainland and northwestern Mongolian clades	Canyon, steppe and river basin	3.17	2.60 [1.15–3.72]	-	ACE – Northern, central to southern ranges: Amur River Basin, southcentral Gobi to Sichuan Basin (29.24%),	Dispersal
11	Southern	Crown clade formation of northern Yangtze river clade	Restricted to lowland forest and river basin	3.14 [1.28–5.60]	2.60 [0.96–4.17]	2.87 [1.12–4.89]	D – Southeastern range – Northern half of Yangtze river (80.20%)	Dispersal

Pattern of gene flow in northeast Asia

The Migrate analysis of the *CR* fragment estimated a high effective population size (Θ) of females among the clades inhabiting the canyons in the southern part of the range (mean Θ = 0.035 [HPD 97.5%: 0.025–0.047]; Table 2; Fig. 4), and the clades inhabiting the steppes of Gobi Desert (mean Θ = 0.035 [HPD 97.5%: 0.022–0.042]; Table 2; Fig. 4). The number of female immigrants per generation (*M*) showed a bidirectional pattern (effective gene flow) in some clades distributed across landscapes. The three effective gene flow events across the landscapes included: (i) from the southern Gobi Desert and the central Mongolian steppes to the Selenge River basin in Mongolia, the Transbaikal and the Amur River Basin (average $M_{\text{steppe to river basin}} = 7.819$; Table 2; Fig. 4) and vice versa (average $M_{\text{river basin to steppe}} = 5.529$; Table 2; Fig. 4), (ii) from the southern Gobi steppes to the canyons of Sichuan Basin, Shanxi and Gansu ($M_{\text{steppe to canyon}} = 4.029$; Table 2; Fig. 4) and vice-versa ($M_{\text{canyon to steppe}} = 2.881$; Table 2; Fig. 4), and (iii) from the Amur river basin to the canyons of the Sichuan Basin ($M_{\text{river basin to canyon}} = 4.723$; Table 2; Fig. 4), and vice-versa ($M_{\text{canyon to river basin}} = 1.834$; Table 2; Fig. 4).

Landscape and genetic barrier

Here, we obtained positive correlations for both geographic distance and landscape connectivity with the genetic structure of *S. raddei* across the range of the species, and for the northern clades specifically (Fig. 5). We determined two significant genetic barriers within East Asia: (i) a longitudinal barrier segregating the populations distributed in the southern area of the species' range, including the Sichuan Basins and northern half of Yangtze river from populations distributed in the central and northern part of the range such as Mongolia and Russia (Bootstrap support 100%; Fig. 5A), (ii) a latitudinal barrier isolating the pre-Tibetan Plateau population of *S. raddei* from other populations within its range (SWC; Bootstrap support 80%; Fig. 5A).

Additionally, the barrier analysis focusing on the four northernmost populations in Mongolia and Russia found a significant barrier located on the Hentiyn Mountains, a section of the Mongolian Plateau ranges. The mountains connect with the Yablonovy range in the Transbaikal area, segregating the northwestern Mongolian populations (northern Gobi) from populations distributed in the river basins of the Baikal, and Amur (NWM; Bootstrap support 80–100%; Fig. 5B).

Furthermore, the Mantel test showed a significant pattern of isolation by distance among the East Asian populations of *S. raddei* (R = 0.144; Fig. 5B). The same positive correlation between genetic and geographic distances was displayed by the northernmost populations of *S. raddei*, particularly the ones distributed in northwestern Russia, northern Mongolia, eastern Mongolia, and the Amur River Basin (R = 0.687; Fig. 5B).

Impact of glaciations on northern clades

The BCSP plot showed an expansion in the population size of the clades originating from the southern part of the range (Clade B) and distributed in northwestern Mongolia and south east of the Baikal (Fig. 6A) during the post-glacial rebound (Fig. 6B). In general, we estimated the expansion of the northern clades (Mongolian and Russian) to

Table 2 Trajectory of migration and estimation of matrilineal gene flow among the *CR* haplotypes for *Strauchbufo Raddei* across its range ($N = 165$). The gene flow represents the rate of female immigrants per generation across the five different clades sorted by landscape types in East Asia. The rates are related to the pattern of migration estimates in Fig. 4

Clade sorted by landscape (i)	Maximum likelihood estimates for population sizes (Θ)			Rate of immigrant females per generation (M/2Nfm)				
	Mean	Profile confidence intervals		Desert grassland $\rightarrow i$	Lowland forest $\rightarrow i$	Canyon $\rightarrow i$	Plateau $\rightarrow i$	River Basin $\rightarrow i$
		25%	97.5%					
Steppe (s)	0.035	0.022	0.042		7.891	2.881	6.478	5.529
Lowland forest (lf)	0.004	0.002	0.007	0.288		0.255	0.286	0.261
Canyon (c)	0.035	0.025	0.047	4.029	6.638		6.748	4.723
Plateau (p)	0.003	0.002	0.005	0.410	0.489	0.285		0.535
River basin (rv)	0.033	0.021	0.040	7.987	7.793	1.834	5.088	

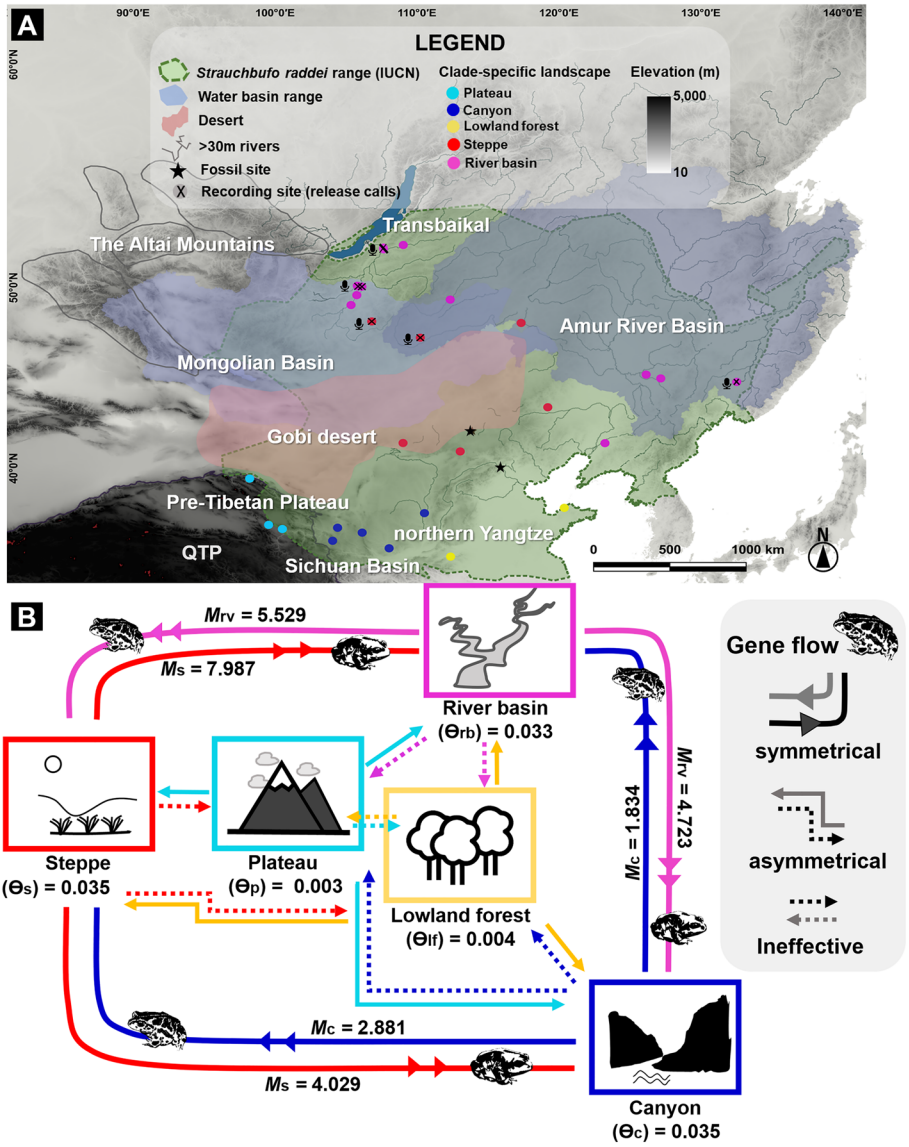

Fig. 4 Migration trajectory among the six clades of *Strauchbufo raddei* assigned to specific landscapes across the species range. **a** Map showing the distribution of each clade within the species range with different landscape features in East Asia. **b** Migration rates and mean theta (Θ) estimates between clades of *S. raddei* distributed across the diverse landscapes of the entire range. The migration rates showed symmetrical gene flow between clades from the Gobi steppes (central range), deep valleys or canyons of the Sichuan Basin (southern range) and Amur River Basin (northeastern range). An asymmetrical gene flow was identified between clades distributed in the pre-Tibetan Plateau (southwestern range) and the northern Yangtze (southeastern range). The 95% credible interval for mean Θ is provided in Table 2

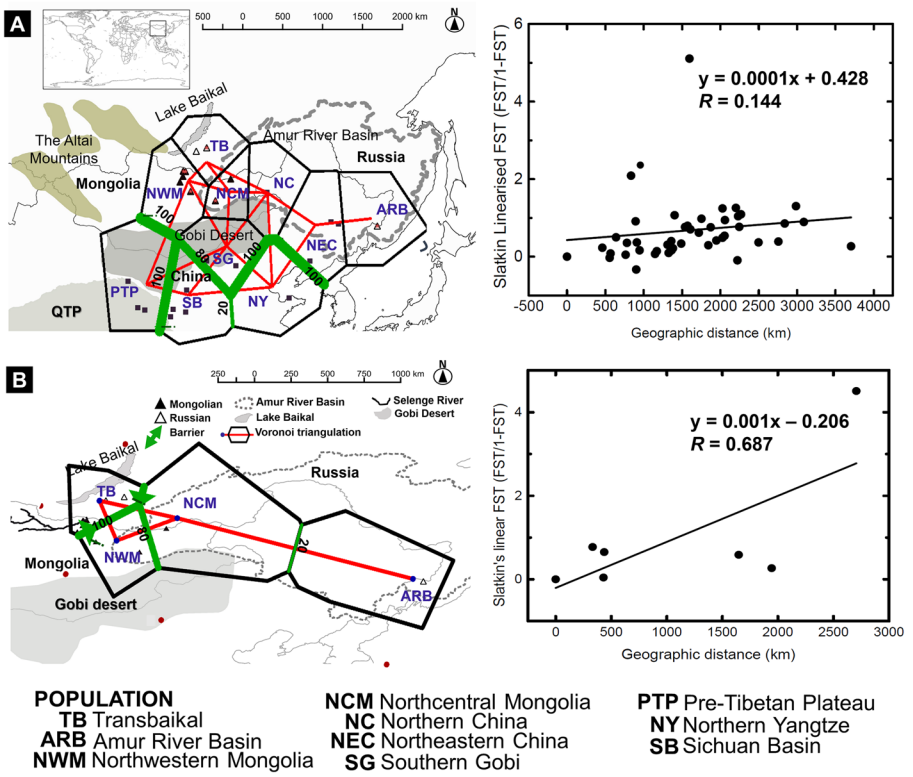

Fig. 5 Landscape barriers and isolation by distance (IBD) for the southern and northern East Asian *Strauchbufo raddei*. The mantel tests inform the IBD, as shown by the correlation between Slatkin's genetic distance (F_{ST} / (1—F_{ST}) versus the geographic distance (km). The most significant landscape barriers to the populations in East Asia are indicated by the green arrow in the Voronoi triangulation on the maps. **a** Mantel test and barrier results for the overall population of *S. raddei*. **b** Mantel test and barrier result for the populations of *S. raddei* restricted to the northern range of the species: Mongolia and Russia. The black and red coloured polygons on maps show external and internal boundaries of the Voronoi cells. Each boundary is computed on the areas of the corresponding cells (blue and red dots) and having equal distance between the cells. The computation is determined using the Euclidean distance functions between the matrices of genetic distances and the distribution sites of *S. raddei*

have occurred as early as the last interglacial (LIG, 0.131 Mya; mean of 3.182; median of 2.256 [Upper to lower HPD 95%: 11.10–0.62]; Fig. 6B). The growth of northern clades then peaked c. 10,500 years before the last glacial period (pre-LGM period; 0.037 Mya; mean of 4.396; median of 3.483 [HPD 95%; 13.828–1.058]; Fig. 6B).

In particular, the population size of the northeastern lineage (Clade A; Fig. 6B) was stagnant since the LIG (250 kya; mean of 410,486.79; median of 354,090.54 [HPD 95%: 1,085,824.33–116,413.53]; Fig. 6C) until the LGM (22 kya, mean of 474,737.46; median of 386,578.98 [HPD 95%: 1,270,600.22–137,330.52; Fig. 6C]. The stagnancy in population growth was then followed by a decline during the Holocene (11 kya; mean of 496,613.87; median of 366,671.53 [HPD 95%: 1,497,474.73–120,179.20]; Fig. 6C). In contrast, we demonstrated an expansion in clades of northwestern Mongolia and Russia (Clade B; Fig. 6D) since the last glacial period (47 kya; mean of 1,181,439.16; median of 482,836.78 [HPD 95%: 5,833,088.45–36,909.95]; Fig. 6D), in which the growth

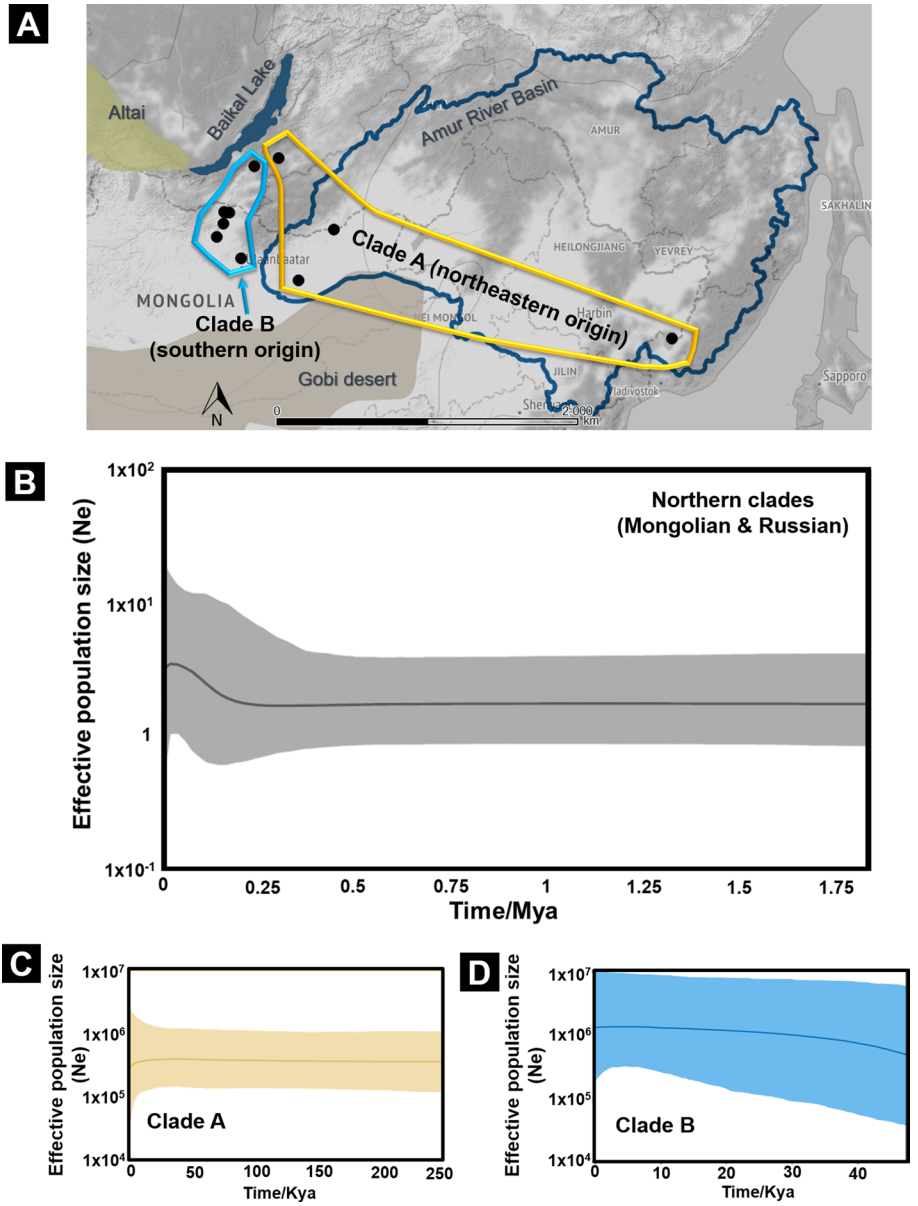

Fig. 6 Bayesian Coalescent Skyline Plots for two divergent clades of *Strauchbufo raddei*. The y-axes indicate the median estimate of effective population size (Ne) and the thin lines and shadows show the mean and boundary of the 95% CPD intervals. The x-axis represents the time between the Last Interglacial (LIG) and present. **a** Distribution of two segregated Clade A and Clade B at the northern limit of species range. **b** Expansion of northern clades since the LIG, peaking during the LGM and declining during the Holocene. **c** Stable growth of Clade A since the LIG and declining during the Holocene. **d** Expansion of Clade B since the LIG and until the last Glacial Maximum (LGM)

accelerated during the LGM (15 kya; mean of 1,907,100.83; median of 1,214,645.33 [HPD 95%: 7,977,727.33–181,780.23]; Fig. 6D), with no sign of decline in population dynamic (present time; mean of 2,239,527.56; median of 1,297,823.30 [HPD 95%: 9,925,896.63–183,636.13]; Fig. 6C).

Release calls variation

We recorded 105 release calls from 29 male individuals (n sites = 4; Fig. 7) with an average call duration of 3.62 ± 0.92 ms (between 2 and 6 calls per individual; Table S2). The call duration, rise time, and fall time were longer in Clade A (east of the Hentiyn Mountains; Table 3; Table 4; Fig. 7) than in Clade B (west of the Hentiyn Mountains; Table 3; Table 4; Fig. 7). The MANOVA test showed a significant variation in release calls (MANOVA;

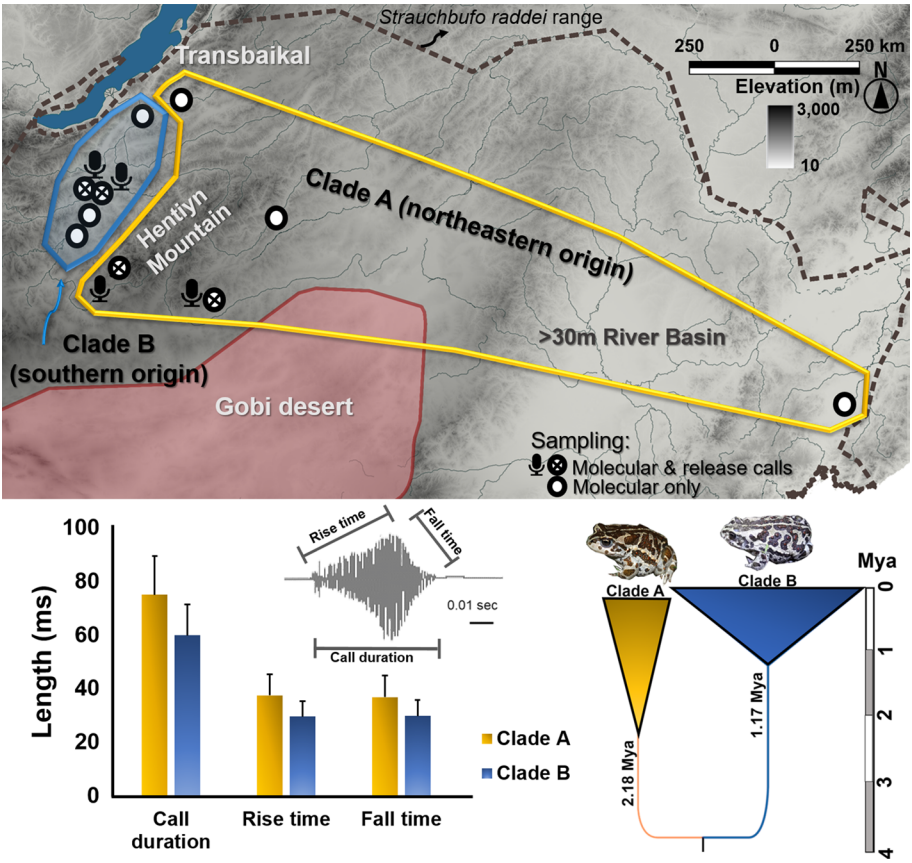

Fig. 7 Oscillogram, tree time and release call characteristics of *Strauchbufo raddei* from two divergent clades. The bar chart shows the geographic variations between the calls of the two lineages: the northeastern clade (orange) and the southern originated clade (blue) in Mongolia and Russia. The colours on the map match with the colours of the bar charts. The release call characteristics that significantly differed between the two clades (call duration, rise time and fall time) are described in the oscillogram

Table 3 Values of call properties and body traits of *Strauchbufo raddei* in different phylogeny clades. The (*) symbol denotes significantly different traits between Clade A and Clade B under MANOVA tests

Individual/call property	Total	Clade A	Clade B	F (1,27)	*p*
N	29	10	19		
Call period (ms)	293 ± 94	273 ± 66	304 ± 105	0.69	0.414
Call duration (ms)*	65 ± 14	75 ± 14	60 ± 12	9.47	0.005
Rise time (ms)*	32 ± 7	38 ± 7	30 ± 6	10.28	0.003
Fall time (ms)*	33 ± 7	38 ± 7	30 ± 6	9.61	0.004
Dominant frequency (Hz)	931 ± 132	930 ± 67	932 ± 158	< 0.01	0.979
SVL (mm)	64.49 ± 7.85	68.6 ± 6.56	62.32 ± 7.75	4.75	0.038
Body condition	0 ± 2.23	-1.03 ± 1.78	0.55 ± 2.29	3.60	0.068

Table 4 Results of MANOVA test using factor score from call properties and body traits of the northern clade of *Strauchbufo raddei* in different phylogeny clades. The (*) symbol demotes significance

Factors	Traits	F (1,27)	*p*
Factor 1*	Call duration, Rise time, Fall time	7.35	0.012
Factor 2	Call period	0.70	0.412
Factor 3	Body condition	2.45	0.129
Factor 4	SVL	2.63	0.116
Factor 5	Dominant frequency	0.07	0.791

Wilk's lambda = 0.52, $F_{(7, 21)} = 2.75$, $p = 0.034$; Table 3) between the clades of northcentral (Clade A) and northwestern Mongolia (Clade B).

Considering the widespread multi-collinearity of these three call traits, we ran a factor analysis to determine the factors influencing the release calls (Table S8). Factor 1 showed a significant difference in the combination of call duration, rise time, and fall time between the two clades (F = 7.35; $p = 0.012$; Table 4), providing support for the variation found in the MANOVA test (Table 4), and matching with the divergence pattern of our Bayesian skyline tree (Fig. 7).

Discussion

We determined the presence of two segregated lineages of *Strauchbufo raddei*, similarly to the pattern found in the Chinese lineages (Dong et al. 2012). However, rather than a western-eastern division (Dong et al. 2012), we refined the origin of each major lineages of *S. raddei* and determined the segregation to be between clades distributed in the north-eastern and southern parts of the species' range (Table 1; Fig. 3). Our dating estimates and the reconstruction of the ancestral range show that the oldest radiation within the north-eastern lineage took place earlier than the radiation of the southern lineage during the Late Miocene (c. 7.14 [4.88−10.44] Mya; Fig. 3) and this radiation may have been the source of emergence for present day *S. raddei* (Table 1; Fig. 3). Our age estimate for the split between the two major *S. raddei* lineages was at least 5 million years older than the previous estimate (c. 2.10 Mya; Dong et al. 2012). However, the comparison between the age estimates of our basal lineages split and the one calculated by Dong et al. (2012) is not

necessarily meaningful as the assignments are based on different molecular divergence estimates. Our study relies on fossil-calibrations, in which we have enforced the Middle Miocene (7–6 Mya) as our minimum age (with lognormally distributed prior) for the basal split between the northeastern and southern lineages. In contrast, Dong et al. (2012) solely enforced a coalescent model with a normally distributed prior for their tree calibration. Here, the timing of our basal splits within the northeastern and southern lineages was also supported by the oldest fossil c. 7.1–5.3 Mya recorded in Inner Mongolia (Böhme and Ilg 2003; Roček et al. 2011). In addition, Dong et al. (2012) included a lower number of taxa as ingroup, mostly representing the Chinese lineage of *S. raddei*, whereas our study combined their Chinese lineage dataset with Mongolia and Russia clades, and likely, also leading to fluctuations in the divergence time estimates.

The early diversification of the northeastern lineage may have been initiated by the aridity-induced vicariance of the northeastern Asian clade in the area south of the Gobi Desert (Table 1; Fig. 3). These results are consistent with the hypothesis stating that the central Asian desertification induced the earliest divergence between Eastern and Western Palearctic common toads, *Bufo* sp. (Othman et al. 2022). In addition, aridity-driven vicariance is not unusual as a speciation mechanisms for steppe dwelling species, and a similar pattern was described for the African lizards genus *Agama* inhabiting the Sahara desert (Gonçalves et al. 2018).

Our data support the remarkable dispersals of *S. raddei* (Dong et al. 2012). The clade currently isolated on the pre-Tibetan Plateau, i.e. southeastern Qinghai, most likely originated from the northeastern lineage and was established through long dispersals over the central and southern areas of the species' range in the Late Pliocene (c. 2.60 Mya; Table 1; Fig. 3). However, we disagree with the previous assumption stating that the eastern lineage colonised the northwestern limit of the range in Mongolia and in the Baikal region (Dong et al. 2012; Litvinchuk et al. 2020). Rather, our results based on a better resolution of the northwestern range of the species provide evidence supporting a southern-originated lineage expansion to northwestern Mongolia and southeastern Baikal. This colonisation likely occurred through northern China and Mongolia, possibly by crossing the steppes of the Gobi Desert (Late Pliocene to Pleistocene; c. 2.60 [1.15–3.72] Mya; Fig. 3).

We highlighted the Pliocene and Pleistocene as the periods of active radiations, resulting in the simultaneous expansion of crown clades in both southern- and northeastern-originated lineages (Table 1; Fig. 3). Similarly, the extensive uplift of the QTP, drastic climatic variations such as the Quaternary climatic oscillations (Othman et al. 2022), sea level fluctuations (Borzée et al. 2017), and the development of the East Asian monsoon system impacted the dry seasons (Yuan et al. 2015), which have led to speciation, population dispersals and fragmentation of many animal taxa in the region (Cheng et al. 2017; Ding et al. 2020).

Despite the strong allopatric structure between the divergent northwestern and north central Mongolian clades, we also found that several *S. raddei* individuals from the Upper Selenge River (northwestern clade) were clustered with the north central Mongolian clade. Natural dispersal is most likely restricted by the natural barrier of the Hentiyn-Yablonovy Mountain range (Fig. 5), and in spite of the limited exchange between populations in intermountain regions, some individuals may share origins with the *S. raddei* from the Hentiyn Mountain range as the maximum altitude is 1700 m above sea levels, i.e. Khangal-Nuur; 48°08′ N, 109°23′ E, 1326 m (Borkin et al. 2011; Kuzmin et al. 2017), and the niche occupied by two mountainous populations are not necessarily distinctive (Goudarzi et al. 2019).

The biogeographic scenarios depicted in the present study are limited by the sole use of mtDNA markers. However, this first phylogeographic inference for S. *raddei* across its

entire range and the study with the largest sample size, variability in geographic locations and diversity in sampling sites. In addition, the *CR* marker is reliable and it is consistently used to support divergence dating estimates in Asian bufonids (Hu et al. 2007; Dong et al. 2012; Yu et al. 2014; Borzée et al. 2017), highlighting the reliability of our result and the genetic diversity in *S. raddei*. Despite the discussion regarding the use of a fixed rate of divergence in *CR* as estimated by Stöck et al. (2006) to calibrate the phylogeny of bufonids (Dufresnes et al. 2019), our preliminary results show that the combination of a fixed rate of divergence and mixed clock models were reliable. The divergence time range provided by the strict clock with the fixed rate model was higher only at the basal node, and the datation of the clades' diversification were mostly consistent with relaxed clock models (Table 1). Additionally, our methodological refinement for the mtDNA gene divergence dating were supported by: (1) primary calibrations sourced from fossils evidence and geological events, (2) comparable biogeography patterns of closely related Asian bufonids species and (3) comparative choice of molecular clocks and tree priors in Bayesian molecular dating, allowing our conclusions to serve as a foundation for future validation using multilocus strategies.

Refugia in northwestern Mongolia

The BCSP plot showed a stable past population dynamic in the northeastern lineage since the last interglacial period (Clade A; Fig. 6C). This result is in agreement with the earlier assumption that Eastern Palearctic *S. raddei* were weakly affected by glaciations (Malakhov 2004; Dong et al. 2012). In comparison, the northwestern Mongolian clade is characterised by a post-glacial expansion of the southern-originated lineage (Clade B; Fig. 6D). This pattern supports the hypothesis of multiple refugia and potential secondary contact with *S. raddei* populations in China (Dong et al. 2012). Northwestern Mongolia was most likely one of the refugia for populations originating from the southern clade (Fig. 6). Plausibly, the species expanded to the northwestern limit of its current range during the post-glacial period (Clade B; Fig. 6D), and became isolated in the western margin of the Hentiyn Mountain range, where the Selenge River Basin provided a refugium. This is reflected by variations in ecological preference, with *S. raddei* inhabiting a wide diversity of landscape and environments, although occurring close to permanent water sources in dry areas such as steppes (Terbish et al. 2006).

We were not inable to secure nuclear data to compare with the mitochondrial results, but we highlights the possible presence of mitonuclear discordance, and especially for the isolated clade originated from the southern lineage and inhabiting new types of habitat (present time northwestern Khentii and Transbaikal). This clade is most likely to have rapidly adapted through radiation (Clade B; Fig. 6), and rapid diversifications in an isolated or refugium population can result to cytonuclear discordance in anurans (Dufresnes et al. 2020).

Effect of mountains barrier

Although distance is playing a role in the divergence between clades in northwestern Mongolia and the southeastern Baikal region, and northern-central Mongolia until the Amur River Basin (Fig. 5B), landscape elements had a larger impact in limiting the genetic connectivity across East Asia (Fig. 5A). The low effective population size for females of the southern clades, with the eastern clade inhabiting lowland forest and the southwestern

clade distributed on the eastern QTP (range of $\Theta = 0.003–0.004$; Table 2; Fig. 4), reflects a high homozygosity resulting from an important genetic drift between those two populations. However, the limited gene flow to the southwestern populations is expected due to the high mountains (Fig. 5), a limitation to connectivity observed in other anurans distributed in the eastern QTP, such as *Kaloula* frogs (Othman et al. 2021). The difference in elevation may also limit the genetic connectivity between the southeastern clade in lowland forests (< 800 m) and the clade in medium to high altitude canyon in Shaanxi and the surrounding areas (1000–2000 m) in northern China.

The Gobi Desert as a receiver of immigration?

The aridification of the Gobi Desert predates the dispersion of *S. raddei* to northwestern Mongolia (Barbolini et al. 2020), and our dating estimates indicate a dispersion over the Gobi Desert as early as the Pliocene, c. 4.36 [2.10–7.02] Mya (Table 1; Fig. 3), during a warmer period than today's climate (Haywood et al. 2016). The colonisation of northern Mongolia by this clade is likely to match with the species' distribution during the last glacial refugia, presumably the present-day northern Gobi, as the divergence time matches with the earliest ice-age c. 2.60 [1.15–3.72] Mya (Table 1; Fig. 3). The time estimates are also consistent with the establishment of the modern Gobi Desert during the Late Pliocene (c.2.6 Mya), when the shift in air surface circulation and the changes in the Asian monsoon due to QTP uplift (Lu et al. 2019) are likely to have driven northward dispersions.

Contrary to the expected effect of grasslands as a barrier to amphibians' dispersion across biomes (Rittenhouse and Semlitsch 2006), the Gobi Desert played the role of a dispersal corridor for the southern-originated clade inhabiting canyons (mountain-range; 1000–2000 m; Fig. 4). Here, we demonstrated that *S. raddei* dispersed across the Gobi Desert, and similar patterns of long-distance dispersion are found in other central Asian desert species (Ito et al. 2006; Kessler et al. 2013). However, it is important to note that the Gobi Desert at the time of dispersal was not as it is currently, which is now a barrier to amphibian dispersion.

Local adaptation

In contrast to most landscape restricted clades in the southwestern area of the species range, we found a weak effect of landscape barriers within the northern populations of *S. raddei*. We detected a high level of gene flow in northern populations across a variety of landscapes including the riverine system of the Baikal Lake and Selenge River, and the steppe and grassland east of the Gobi Desert (Fig. 4). Hence, the weaker impact of ice age glaciations on East Asia is not the only explanation for the survival of *S. raddei* in the region. A combination of factors such as variation in ecological characteristics, dispersal capacity and habitat preference might have contributed to the genetic diversity of the clades, which may have helped modern Asian *S. raddei* adapt and survive in several biotopes (Lei et al. 2014). Similarly, a high genetic diversity also facilitated the survival of the Italian *B. bufo* during the Pleistocene climatic oscillations (Chiocchio et al. 2021).

Extreme environments tend to promote local adaptation in bufonids (Luquet et al. 2015; Yu et al. 2019). Due to their limited dispersal ability over high physical barriers (Cayuela et al. 2020), the *S. raddei* clades isolated in the pre-Tibetan Plateau (southwestern China) had to adapt to high-altitude habitat (Yu and Lu 2012). Similarly, while herpetological diversity in deserts is low due to high temperature and aridity, and especially in

Mongolia (Munkhbayar and Munkhbaatar 2012), *S. raddei* is distributed over the Gobi Desert (Fig. 4). The clade has adapted to the environmental conditions and predations in grassland, as testified by its specialised morphology and skeleton (Kuzmin and Ischenko 1997) and its specific escape behaviour from predators. The resistance to other landscape features generally detrimental to amphibians, such as water conductivity further supports the behavioural and physiological adaptation of *S. raddei* (Borzée et al. 2021a).

Additionally, the potential adaptive introgression with extinct species highly similar to *S. raddei* (Syromyatnikova 2015) could have facilitated the adaptability of *S. raddei* to diverse biotopes. Adaptive introgression with 'ghost' species is not uncommon in species adapted to extreme conditions, such as the high-altitude of the QTP (Wang et al. 2020).

Release calls as a signal of demographic history?

In opposition to previous findings showing that the structure of release calls is not phylogeographically informed in *Pelobates* toads (Stănescu et al. 2019), our results provide evidence of variation in release calls between the two focal northern clades (Fig. 7). In previous studies, advertisement calls were the call type generally matching with phylogenetic lineages (Jang et al. 2011; Borzée et al. 2020), and they are critical for individuals to identify conspecific animals (Chuang et al. 2016). This type of premating isolation results from advertisement calls being under sexual selection, which is not the case for release calls. However, the phylogenetic segregation of release calls in this study is matching with the pattern of post-glacial expansion found in the northwestern clades (Clade B; Fig. 6D).

Our data provided support in the importance of phylogenetic variables for acoustic traits (Forti et al. 2017). Males of Clade A had a significantly higher call duration, rise time and fall time than those of Clade B (Fig. 7), indicating that the two clades have segregated phenotypic and behavioural traits, most likely related to the environment and landscapes. The segregation in release calls shows that the northwestern *S. raddei* clade dispersed to the northern refugium and became isolated in the moist steppe of the Selenge River and Baikal Lake on the western side of the Hentyin Mountains (Fig. 7).

Conclusions

Our biogeographic reconstruction for the Mongolian toad *Strauchbufo raddei* across the species range resolved the pattern of emergence into the Eastern Palearctic c. 11.63 Mya, followed by the separation between northeastern and southern lineages. We highlighted that the radiation within the northeastern lineage likely resulted from a desertification-induced vicariance in the northern Gobi in the Late Miocene, c. 10.00–7.14 Mya, followed by dispersals across the central and southern parts of the species range in the Plio-Pleistocene. Subsequently, vicariance and dispersal triggered the emergence of the southern lineage in the Sichuan Basin c. 6.84–2.63 Mya. We found a significant impact of the northern glacial refugia within the southern lineage, as the clades inhabiting the Sichuan Basin may have colonised the steppes of the Gobi 6.84 [3.48−2.63] Mya and expanded into northwestern Mongolia during the earliest ice age. We emphasised the presence of effective gene flow within the northeastern lineage, especially in clades inhabiting the steppes of the Gobi, Sichuan canyons and Amur River Basin. In contrast, the mountainous range of the pre-Tibetan Plateau and forested landscapes of the northern Yangtze may have restricted the migration of clades in the southwestern and southeastern sections of *S. raddei* range.

Through comparative population dynamics, acoustic analysis and phylogeographic resolution focusing on the northern clades, we clarified that the northern glacial refugia contributed to the allopatric separation in release calls between the populations distributed across the western and eastern margins of the Hentiyn Mountains in Mongolia.

Supplementary Information The online version contains supplementary material available at https://doi.org/10.1007/s10682-022-10206-4.

Acknowledgements The authors are grateful to Erdenetushig Purvee, Tumenkheslen Munkhsaikhan and Solongo Gansukh from the Mongolian State University of Education for their supports during sample collection. The authors also acknowledge the help provided by Yury Evgenyevich Dochevoy, Ye Inn Kim, Sungsik Kong, Yoonjung Yi, Kyungmin Kim and Desiree Andersen in the field. We thank Kevin R. Messenger for the use of *Strauchbufo raddei* photos in Figs. 4 and 7.

Authors contributions SNO and AB conceived the idea, YJ evaluated the idea and validated the data. MC, AB, IM and NAS involved in data collection. MC conducted the experiments and analysed the data, SNO analysed and interpreted the bioinformatics data. MFC analysed the acoustic data, MC and AB supported the data analyses. SNO wrote the first draft of the manuscript and MC supported the writing. All authors were involved in the revision of the manuscript and AB improved the draft to its final version.

Funding This project was financially funded by Rural Development Administration of Korea grant (PJ015071) and Korea's Environmental Industry and Technology Institute under a project entitled 'Development of behavioural ecological methods for population regulation of invasive amphibians and reptiles' (Step 2) under the grant number KEITI 2021002270001 to YJ. This project was also supported by the Foreign Youth Talent Program (QN2021014013L) from the Ministry of Science and Technology of People's Republic of China to AB, and partially supported by the Dobretsov Cenozoic Geology Laboratory of the Geological Institute of the SB RAS (AAAA-A21-121011390004–6) to NAS.

Data availability The supporting data of this study is available as supplementary information. The BEAST codes (.xml) generated for molecular dating analyses are available in Mendeley database http://dx.doi.org/10.17632/jsjfww4rg2.1 and can be cited as Othman, S. N. (2021), "Across the Gobi Desert: impact of landscape features on the phylogeography and release calls of the Mongolian Toad *Strauchbufo raddei* in East Asia", Mendeley Data, V1, http://dx.doi.org/10.17632/jsjfww4rg2.1.

Declarations

Conflict of interest The authors declared no conflict of interest regarding the publication of this article. First co-author Minjee Choe is entitled to claim this study as the first author in her curriculum vitae.

Ethical approval Samplings in Mongolia were conducted under a research permit J22962. The study and general sampling followed the ethical requirements and regulations of Experimental Animal Welfare and Ethics Committee of Nanjing Forestry University under IACUC approval (permit number 2022011). To ensure non-invasive genetic sampling, all individuals found alive were orally swabbed (Dryswab™ ENT, Medical Wire, Wiltshire, UK) and they were released at the point of capture based on the methodological standard of Broquet et al. (2007). Release call samples were recorded without the harm on the animals and treated with humane care based on the methodological guidelines provided by Animal Behaviour Society 2018 (Animal Behaviour Society 2018) and Chuang et al. (2016). In-situ experiments and data processing such as bioinformatics and bio statistical analyses were partially conducted in Ewha Womans University, Republic of Korea, and they did not require an IACUC permit, in accord to the rules of EWHA Institutional Biosafety Committee (IBC).

References

Adams RV, Lazerte SE, Otter KA, Burg TM (2016) Influence of landscape features on the microgeographic genetic structure of a resident songbird. Heredity 117:63–72. https://doi.org/10.1038/hdy.2016.12

Andren H (1994) Effects of habitat fragmentation on birds and mammals in landscapes with different proportions of suitable habitat : a review. Oikos 71:355–366
Animal Behaviour Society (2018) Guidelines for the treatment of animals in behavioural research and teaching. Animal Behaviour https://doi.org/10.1016/j.anbehav.2017.10.001
Barbolini N, Woutersen A, Dupont-Nivet G et al (2020) Cenozoic evolution of the steppe-desert biome in Central Asia. Sci Adv 6:1–17. https://doi.org/10.1126/sciadv.abb8227
Bartelt PE, Klaver RW (2017) Response of anurans to wetland restoration on a midwestern agricultural landscape. J Herpetol 51:504–514. https://doi.org/10.1670/16-113
Barton NH, Turelli M (1987) Adaptive landscapes, genetic distance and the evolution of quantitative characters. Genet Res 49:157–173. https://doi.org/10.1017/S0016672300026951
Beerli P, Mashayekhi S, Sadeghi M et al (2019) Population Genetic Inference With MIGRATE. Curr Protoc Bioinformatics 68:1–28. https://doi.org/10.1002/cpbi.87
Biggs J, Williams P, Whitfield M et al (2005) 15 years of pond assessment in Britain: results and lessons learned from the work of pond conservation. Aquat Conserv Mar Freshwat Ecosyst 15:693–714. https://doi.org/10.1002/aqc.745
Bletsa M, Suchard MA, Ji X et al (2019) Divergence dating using mixed effects clock modelling: an application to HIV-1. Virus Evol. https://doi.org/10.1093/ve/vez036
Böhme M, Ilg A (2003) fosFARbase. www.wahre-staerke.com/. Accessed 15 Aug 2020
Borkin LJ, Litvinchuk SN, Munkhbayar K, et al (2011) Amphibians and reptiles of eastern Mongolia (some results of the joint Russian-Mongolian herpetological expedition, 2008). In: Ananjeva NB, editor. Problems of herpetology. St. Petersburg: Zoological Institute of RAS, pp 36–47
Borzée A, Santos JL, Sánchez-RamÍrez S et al (2017) Phylogeographic and population insights of the Asian common toad (*Bufo gargarizans*) in Korea and China: population isolation and expansions as response to the ice ages. PeerJ 5:e4044. https://doi.org/10.7717/peerj.4044
Borzée A, Messenger KR, Chae S et al (2020) Yellow sea mediated segregation between North East Asian *Dryophytes* species. PLoS ONE 15:e0234299. https://doi.org/10.1371/journal.pone.0234299
Borzée A, Kim YI, Purevdorj Z et al (2021a) Relationship between anuran larvae occurrence and aquatic environment in septentrional east Palearctic landscapes. Herpetozoa 34:265–270. https://doi.org/10.3897/herpetozoa.34.e68577
Borzée A, Litvinchuk SN, Ri K et al (2021b) Update on distribution and conservation status of amphibians in the democratic people's republic of Korea: conclusions based on field surveys, environmental modelling, molecular analyses and call properties. Animals 11:2057. https://doi.org/10.3390/ani11072057
Bouckaert RR, Drummond AJ (2017) bModelTest: bayesian phylogenetic site model averaging and model comparison. BMC Evol Biol 17:1–11. https://doi.org/10.1186/s12862-017-0890-6
Bouckaert R, Vaughan TG, Barido-Sottani J et al (2019) BEAST 2.5: an advanced software platform for Bayesian evolutionary analysis. PLoS Comput Biol 15:1006650. https://doi.org/10.1371/journal.pcbi.1006650
Broquet T, Berset-Braendli L, Emaresi G, Fumagalli L (2007) Buccal swabs allow efficient and reliable microsatellite genotyping in amphibians. Conserv Genet 8:509–511. https://doi.org/10.1007/s10592-006-9180-3
Castellano S, Tontini L, Giacoma C et al (2002) The evolution of release and advertisement calls in green toads (*Bufo viridis* complex). Biol J Lin Soc 77:379–391. https://doi.org/10.1046/j.1095-8312.2002.00118.x
Cayuela H, Valenzuela-Sánchez A, Teulier L et al (2020) Determinants and consequences of dispersal in vertebrates with complex life cycles: a review of pond-breeding amphibians. Q R Biol 95:1–36. https://doi.org/10.1086/707862
Cheng J, Lv X, Xia L et al (2017) Impact of orogeny and environmental change on genetic divergence and demographic history of Dipus sagitta (Dipodoidea, Dipodinae) since the Pliocene in inland East Asia. J Mamm Evol 26:253–266. https://doi.org/10.1007/s10914-017-9397-6
Chiocchio A, Arntzen JW, Martínez-Solano I et al (2021) Reconstructing hotspots of genetic diversity from glacial refugia and subsequent dispersal in Italian common toads (*Bufo bufo*). Sci Rep 11:260. https://doi.org/10.1038/s41598-020-79046-y
Chuang MF, Kam YC, Bee MA (2016) Quantitative description of the vocal repertoire of the territorial olive frog *Babina adenopleura* from Taiwan. Bioacoustics 25:1–18. https://doi.org/10.1080/09524622.2015.1076347
Clark PU, Dyke AS, Shakun JD et al (2009) The last glacial maximum. Science 325:710–714. https://doi.org/10.1126/science.1172873
Corp S (2017) Stata statistical software: release 15. StataCorp LLC, College Station, TX

Ding L, Liao J, Liu N (2020) The uplift of the Qinghai-Tibet Plateau and glacial oscillations triggered the diversification of *Tetraogallus* (Galliformes, Phasianidae). Ecol Evol 10:1722–1736. https://doi.org/10.1002/ece3.6008

Dong B, Che J, Ding L et al (2012) Testing hypotheses of Pleistocene population history using coalescent simulations: refugial isolation and secondary contact in *Pseudepidalea raddei* (amphibia: Bufonidae). Asian Herpetol Res 3:103–113. https://doi.org/10.3724/SP.J.1245.2012.00103

Drummond AJ, Rambaut A, Shapiro B, Pybus OG (2005) Bayesian coalescent inference of past population dynamics from molecular sequences. Mol Biol Evol 22:1185–1192. https://doi.org/10.1093/molbev/msi103

Dufresnes C, Mazepa G, Jablonski D et al (2019) Fifteen shades of green: the evolution of *Bufotes* toads revisited. Mol Phylogenet Evol 141:106615. https://doi.org/10.1016/j.ympev.2019.106615

Dufresnes C, Nicieza AG, Litvinchuk SN et al (2020) Are glacial refugia hotspots of speciation and cytonuclear discordances? Answers from the genomic phylogeography of Spanish common frogs. Mol Ecol 29:986–1000. https://doi.org/10.1111/mec.15368

Excoffier L, Lischer HEL (2010) Arlequin suite ver 3.5: a new series of programs to perform population genetics analyses under Linux and Windows. Mol Ecol Resour 10:564–567. https://doi.org/10.1111/j.1755-0998.2010.02847.x

Favre A, Päckert M, Pauls SU et al (2015) The role of the uplift of the Qinghai-Tibetan Plateau for the evolution of Tibetan biotas. Biol Rev Camb Philos Soc 90:236–253. https://doi.org/10.1111/brv.12107

Fong JJ, Yang BT, Li PP et al (2020) Phylogenetic systematics of the Water Toad (*Bufo stejnegeri*) elucidates the evolution of semi-aquatic toad ecology and Pleistocene glacial refugia. Front Ecol Evol 7:523. https://doi.org/10.3389/fevo.2019.00523

Forti LR, Lingnau R, Encarnação LC et al (2017) Can treefrog phylogeographical clades and species' phylogenetic topologies be recovered by bioacoustical analyses? PLoS ONE 12:e0169911. https://doi.org/10.1371/journal.pone.0169911

Fu YX (1997) Statistical tests of neutrality of mutations against population growth, hitchhiking and background selection. Genetics 147:915–925

Fu J (1999) Phylogeny of Lacertid Lizards (Squamata: Lacertidae) and the evolution of unisexuality. Univ. of Toronto, Toronto

Garcia-Porta J, Litvinchuk SN, Crochet PA et al (2012) Molecular phylogenetics and historical biogeography of the west-palearctic common toads (*Bufo bufo* species complex). Mol Phylogenet Evol 63:113–130. https://doi.org/10.1016/j.ympev.2011.12.019

Goigel M, Turner MG (1989) Landscape ecology: the effect of pattern on process. Annu Rev Ecol Syst 20:171–197

Gonçalves DV, Pereira P, Velo-Antón G et al (2018) Assessing the role of aridity-induced vicariance and ecological divergence in species diversification in North-West Africa using *Agama* lizards. Biol J Lin Soc 124:363–380. https://doi.org/10.1093/biolinnean/bly055

Goudarzi F, Hemami MR, Rancilhac L et al (2019) Geographic separation and genetic differentiation of populations are not coupled with niche differentiation in threatened Kaiser's spotted newt (Neurergus kaiseri). Sci Rep 9:6239. https://doi.org/10.1038/s41598-019-41886-8

Haywood AM, Dowsett HJ, Dolan AM (2016) Integrating geological archives and climate models for the mid-Pliocene warm period. Nat Commun 7:10646. https://doi.org/10.1038/ncomms10646

Homola JJ, Loftin CS, Kinnison MT (2019) Landscape genetics reveals unique and shared effects of urbanization for two sympatric pool-breeding amphibians. Ecol Evol 9:11799–11823. https://doi.org/10.1002/ece3.5685

Hu YL, Wu XB, Jiang ZG et al (2007) Population genetics and phylogeography of *Bufo gargarizans* in China. Biochem Genet 45:697–711. https://doi.org/10.1007/s10528-007-9107-9

Igawa T, Oumi S, Katsuren S, Sumida M (2013) Population structure and landscape genetics of two endangered frog species of genus *Odorrana*: Different scenarios on two islands. Heredity 110:46–56. https://doi.org/10.1038/hdy.2012.59

Ito TY, Miura N, Lhagvasuren B et al (2006) Satellite tracking of Mongolian gazelles (*Procapra gutturosa*) and habitat shifts in their seasonal ranges. J Zool 269:291–298. https://doi.org/10.1111/j.1469-7998.2006.00077.x

Jang Y, Hahm EH, Lee HJ et al (2011) Geographic variation in advertisement calls in a tree frog species: Gene flow and selection hypotheses. PLoS ONE 6:e23297. https://doi.org/10.1371/journal.pone.0023297

Joly P (2019) Behavior in a changing landscape: using movement ecology to inform the conservation of pond-breeding amphibians. Front Ecol Evol 7:155. https://doi.org/10.3389/fevo.2019.00155

Jukes TH, Cantor CR (1969) Evolution of protein molecules. Mamm Prot Metab 3:21–132

Katayama N, Amano T, Naoe S et al (2014) Landscape heterogeneity-biodiversity relationship: Effect of range size. PLoS ONE 9:e93359. https://doi.org/10.1007/978-981-10-5041-1_31

Kearse M, Moir R, Wilson A et al (2012) Geneious Basic: an integrated and extendable desktop software platform for the organization and analysis of sequence data. Bioinformatics 28:1647–1649. https://doi.org/10.1093/bioinformatics/bts199

Kent M (2007) Biogeography and landscape ecology. Prog Phys Geogr 31:345–355. https://doi.org/10.1177/0309133307079059

Kessler AE, Batbayar N, Natsagdorj T et al (2013) Satellite telemetry reveals long-distance migration in the Asian great bustard *Otis tarda dybowskii*. J Avian Biol 44:311–320. https://doi.org/10.1111/j.1600-048X.2013.00072.x

Kimura M (1980) Evolutionary rates models. J Mol Evol 16:111–120. https://doi.org/10.1007/BF01731581

Knutson MG, Sauer JR, Olsen DA et al (1999) Effects of landscape composition and wetland fragmentation on frog and toad abundance and species richness in Iowa and Wisconsin, U.S.A. Conserv Biol 13:1437–1446. https://doi.org/10.1046/j.1523-1739.1999.98445.x

Kocher TD, Thomas WK, Meyer A et al (1989) Dynamics of mitochondrial DNA evolution in animals: amplification and sequencing with conserved primers. Proc Natl Acad Sci USA 86:6196–6200. https://doi.org/10.1073/pnas.86.16.6196

Köhler J, Jansen M, Rodríguez A, et al (2017) The use of bioacoustics in anuran taxonomy: Theory, terminology, methods and recommendations for best practice

Kuzmin SL, Ischenko VG (1997) Skeletochronology of *Bufo raddei* from the Gobi Desert. J Herpetol 31:306–309

Kuzmin SL, Dunayev E, Munkhbayar K et al (2017) The amphibians of mongolia, 2nd edn. KMK Scientific Press, Moscow

Kuzmin S, Matsui M, Gang L, Maslova I (2004) *Strauchbufo raddei*. The IUCN Red List of Threatened Species 8235:e.T54744A11198066

Landis MJ, Matzke NJ, Moore BR, Huelsenbeck JP (2013) Bayesian analysis of biogeography when the number of areas is large. Syst Biol 62:789–804. https://doi.org/10.1093/sysbio/syt040

Lanfear R, Frandsen PB, Wright AM et al (2017) Partitionfinder 2: new methods for selecting partitioned models of evolution for molecular and morphological phylogenetic analyses. Mol Biol Evol 34:772–773. https://doi.org/10.1093/molbev/msw260

Larkin MA, Blackshields G, Brown NP et al (2007) Clustal W and Clustal X version 2.0. Bioinformatics 23:2947–2948. https://doi.org/10.1093/bioinformatics/btm404

Lee KH, Shaner PJL, Lin YP, Lin SM (2016) Geographic variation in advertisement calls of a Microhylid frog - testing the role of drift and ecology. Ecol Evol 6:3289–3298. https://doi.org/10.1002/ece3.2116

Lei F, Qu Y, Song G (2014) Species diversification and phylogeographical patterns of birds in response to the uplift of the qinghai-tibet plateau and quaternary glaciations. Curr Zool 60:149–161. https://doi.org/10.1093/czoolo/60.2.149

Leigh JW, Bryant D (2015) POPART: full-feature software for haplotype network construction. Methods Ecol Evol 6:1110–1116. https://doi.org/10.1111/2041-210X.12410

Li Z, Yu G, Rao D, Yang J (2012) Phylogeography and demographic history of Babina pleuraden (Anura, ranidae) in Southwestern China. PLoS ONE 7:e34013. https://doi.org/10.1371/journal.pone.0034013

Li JJ, Hu ZM, Sun ZM et al (2017) Historical isolation and contemporary gene flow drive population diversity of the brown alga *Sargassum thunbergii* along the coast of China. BMC Evol Biol 17:246. https://doi.org/10.1186/s12862-017-1089-6

Li B, Zhang W, Wang Z et al (2020) Effects of landscape heterogeneity and breeding habitat diversity on rice frog abundance and body condition in agricultural landscapes of Yangtze River Delta, China. Curr Zool 66:615–623. https://doi.org/10.1093/CZ/ZOAA025

Librado P, Rozas J (2009) DnaSP v5: a software for comprehensive analysis of DNA polymorphism data. Bioinformatics 25:1451–1452

Litvinchuk SN, Schepina NA, Borzée A (2020) Reconstruction of past distribution for the Mongolian toad, *Strauchbufo raddei* (Anura: Bufonidae) using environmental modeling. Peer J 8:e9216. https://doi.org/10.7717/peerj.9216

Liu W, Lathrop A, Fu J et al (2000) Phylogeny of East Asian bufonids inferred from mitochondrial DNA sequences (Anura: Amphibia). Mol Phylogenet Evol 14:423–435. https://doi.org/10.1006/mpev.1999.0716

Liu Z, Yao Z, Wang R, Yu G (2020) Estimation of the Qinghai-Tibetan Plateau runoff and its contribution to large Asian rivers. Sci Total Environ 749:141570. https://doi.org/10.1016/j.scitotenv.2020.141570

Lu H, Wang X, Wang X et al (2019) Formation and evolution of desert-Gobi in central and eastern Asia. Earth Sci Rev 194:251–263. https://doi.org/10.1016/j.earscirev.2019.04.014

Luquet E, Léna JP, Miaud C, Plénet S (2015) Phenotypic divergence of the common toad (*Bufo bufo*) along an altitudinal gradient: Evidence for local adaptation. Heredity 114:69–79. https://doi.org/10.1038/hdy.2014.71

Malakhov DV (2004) Toads (Anura, Bufonidae) from the middle miocene in the Turgay depression (Central Kazakhstan). Biota 5:41–46

Mângia S, Camurugi F, Pereira EA et al (2019) Release calls of four species of Phyllomedusidae (Amphibia, Anura). Herpetozoa 32:77–81. https://doi.org/10.3897/herpetozoa.32.e35729

Manni F, Guérard E, Heyer E (2004) Geographic patterns of (genetic, morphologic, linguistic) variation: how barriers can be detected by using Monmonier's algorithm. Hum Biol 76:173–190. https://doi.org/10.1353/hub.2004.0034

Monmonier M (1989) Geographic brushing: enhancing exploratory analysis of the scatterplot matrix. Geogr Anal 21:81–84. https://doi.org/10.1111/j.1538-4632.1989.tb00879.x

Mott CL (2010) Environmental constraints to the geographic expansion of plant and animal species. Nat Educ Knowl 3:72

Munkhbayar K, Munkhbaatar M (2012) Herpetological diversity of Mongolia and its conservation issues. Erforschung biologischer Ressourcen der Mongolei/ Exploration into the Biological Resources of Mongolia 12:203–212

Okamiya H, Kusano T (2019) Effects of landscape features on gene flow among urban frog populations. Ecol Res 34:497–508. https://doi.org/10.1111/1440-1703.12011

Othman SN, Chen Y-H, Chuang M-F et al (2020) Impact of the Mid-Pleistocene Revolution and anthropogenic factors on the dispersion of Asian Black-spined toads (*Duttaphrynus melanostictus*). Animals 10:1157. https://doi.org/10.3390/ani10071157

Othman SN, Putri ET, Messenger KR et al (2021) Impact of the Miocene orogenesis on *Kaloula* spp. radiation, and implication of local refugia on genetic diversification. Integrative Zoology 17:261–284. https://doi.org/10.1111/1749-4877.12538

Othman SN, Litvinchuk SN, Maslova I, et al (2022) From Gondwana to the Yellow Sea, evolutionary diversifications of true toads *Bufo* sp. in the Eastern Palearctic and a revisit of species boundaries for Asian lineages. eLife Sciences 11:e70494. https://doi.org/10.7554/eLife.70494

Palumbi SR (1996) What can molecular genetics contribute to marine biogeography? An urchin's tale. J Exp Mar Biol Ecol 203:75–92. https://doi.org/10.1016/0022-0981(96)02571-3

Price RM, Meyer ER (1979) An Amplexus Call Made by the Male American Toad, *Bufo americanus americanus* (Amphibia, Anura, Bufonidae). J Herpetol 13:506. https://doi.org/10.2307/1563489

Pröhl H, Ron SR, Ryan MJ (2010) Ecological and genetic divergence between two lineages of Middle American túngara frogs *Physalaemus* (=*Engystomops*) *pustulosus*. BMC Evol Biol 10:146. https://doi.org/10.1186/1471-2148-10-146

Rambaut A, Drummond AJ, Xie D et al (2018) Posterior summarization in Bayesian phylogenetics using Tracer 1.7. Syst Biol 67:901–904. https://doi.org/10.1093/sysbio/syy032

Ratnikov VY (2001) Osteology of Russian toads and frogs for paleontological researches. Acta Zoologica Cracoviensia 44:1–23

Ratnikov VY (2016) Dynamics of East European modern amphibian and reptile species distribution areas and their potential use in Quaternary stratigraphy. CR Palevol 15:721–730. https://doi.org/10.1016/j.crpv.2015.08.003

Reichert MS, Höbel G (2018) Phenotypic integration and the evolution of signal repertoires: a case study of treefrog acoustic communication. Ecol Evol 8:3410–3429. https://doi.org/10.1002/ece3.3927

Rittenhouse TAG, Semlitsch RD (2006) Grasslands as movement barriers for a forest-associated salamander: migration behavior of adult and juvenile salamanders at a distinct habitat edge. Biol Cons 131:14–22. https://doi.org/10.1016/j.biocon.2006.01.024

Roček Z, Dong L, Přikryl T et al (2011) Fossil frogs (Anura) from Shanwang (Middle Miocene; Shandong Province, China). Geobios 44:499–518. https://doi.org/10.1016/j.geobios.2010.11.009

Ronquist F, Teslenko M, Van Der Mark P et al (2012) Mrbayes 3.2: efficient bayesian phylogenetic inference and model choice across a large model space. Syst Biol 61:539–542. https://doi.org/10.1093/sysbio/sys029

Ryan MJ, Cocroft RB, Wilczynski W (1990) The role of environmental selection in intraspecific divergence of mate recognition signals in the Cricket Frog. Acris Crepit Evol 44:1869

Seifert E (2014) OriginPro 9.1: Scientific data analysis and graphing software - Software review. J Chem Inf Model 54:1552. https://doi.org/10.1021/ci500161d

Stănescu F, Forti LR, Cogălniceanu D, Márquez R (2019) Release and distress calls in European spadefoot toads, genus *Pelobates*. Bioacoustics 28:224–238. https://doi.org/10.1080/09524622.2018.1428116

Stöck M, Moritz C, Hickerson M et al (2006) Evolution of mitochondrial relationships and biogeography of Palearctic green toads (*Bufo viridis* subgroup) with insights in their genomic plasticity. Mol Phylogenet Evol 41:663–689. https://doi.org/10.1016/j.ympev.2006.05.026

Strauch A (1876) Otdiel' III. Presm'ikaiushchiiasia i Zemnodn'iia. Mongoliia i strana tangutov; trechletnee puteshestvieh v voctochnoi Nagornii Azii [= Mongolia and the Tangut Country: A Three Years' Journey in the Eastern Highlands of Asia]

Syromyatnikova EV (2015) A new species of *Bufo* (Amphibia, anura) from the Miocene of Russia. Russ J Herpetol 22:281–288

Tajima F (1989) Statistical method for testing the neutral mutation hypothesis by DNA polymorphism. Genetics 123:585–595

Tamura K, Nei M (1993) Estimation of the number of nucleotide substitutions in the control region of mitochondrial DNA in humans and chimpanzees. Mol Biol Evol 10:512–526. https://doi.org/10.1093/oxfordjournals.molbev.a040023

Terbish K, Munkhbayar K, Clark EL, et al (2006) Mongolian red list of reptiles and amphibians. London

Varin C, Reid N, Firth D (2011) An overview of composite likelihood methods. Stat Sin 21:5–42

Wang Y, Lane A, Ding P (2012) Sex-biased dispersal of a frog (*Odorrana schmackeri*) is affected by patch isolation and resource limitation in a fragmented landscape. PLoS ONE 7:e47683. https://doi.org/10.1371/journal.pone.0047683

Wang MS, Wang S, Li Y et al (2020) Ancient hybridization with an unknown population facilitated high-altitude adaptation of canids. Mol Biol Evol 37:2616–2629. https://doi.org/10.1093/molbev/msaa113

White RH, Battisti DS, Roe GH (2017) Mongolian mountains matter most: Impacts of the latitude and height of asian orography on pacific wintertime atmospheric circulation. J Clim 30:4065–4082. https://doi.org/10.1175/JCLI-D-16-0401.1

Xing Y, Ree RH (2017) Uplift-driven diversification in the Hengduan Mountains, a temperate biodiversity hotspot. Proc Natl Acad Sci USA 114:E3444–E3451. https://doi.org/10.1073/pnas.1616063114

Yu TL, Lu X (2012) Mating patterns of *Bufo raddei* from three high altitude populations in southwestern China. Herpetol J 22:213–217

Yu TL, Du LH, Weng CF (2014) A new phylogeographic pattern of endemic *Bufo bankorensis* in Taiwan Island is attributed to the genetic variation of populations. PLoS ONE 9:e98029. https://doi.org/10.1371/journal.pone.0098029

Yu Y, Harris AJ, Blair C, He X (2015) RASP (Reconstruct Ancestral State in Phylogenies): a tool for historical biogeography. Mol Phylogenet Evol 87:46–49. https://doi.org/10.1016/j.ympev.2015.03.008

Yu TL, Wang DL, Busam M, Deng YH (2019) Altitudinal variation in body size in *Bufo minshanicus* supports Bergmann's rule. Evol Ecol 33:449–460. https://doi.org/10.1007/s10682-019-09984-1

Yuan ML, Zhang QL, Wang ZF et al (2015) Molecular phylogeny of grassland caterpillars (Lepidoptera: Lymantriinae: *Gynaephora*) endemic to the Qinghai-Tibetan plateau. PLoS ONE 10:e0127257. https://doi.org/10.1371/journal.pone.0127257

Authors and Affiliations

Siti N. Othman[1] · Minjee Choe[2] · Ming-Feng Chuang[3] · Zoljargal Purevdorj[4] · Irina Maslova[5] · Natalya Alekseevna Schepina[6] · Yikweon Jang[2] · Amaël Borzée[1]

✉ Yikweon Jang
jangy@ewha.ac.kr

✉ Amaël Borzée
amaelborzee@gmail.com

Siti N. Othman
dy.othman@gmail.com

Minjee Choe
minjeechoe@gmail.com

Ming-Feng Chuang
adammfc@gmail.com

Zoljargal Purevdorj
zoljargal@msue.edu.mn

Irina Maslova
irinarana@yandex.ru

Natalya Alekseevna Schepina
natschepina@rambler.ru

[1] Laboratory of Animal Behaviour and Conservation, College of Biology and the Environment, Nanjing Forestry University, 159 Longpan Rd, Nanjing, Jiangsu, People's Republic of China

[2] Department of Life Sciences and Division of EcoScience, Ewha Womans University, Seoul, Republic of Korea

[3] Department of Life Sciences and Research Center for Global Change Biology, National Chung Hsing University, Taichung 402, Taiwan

[4] Department of Biology, School of Natural Science, Mongolian State University of Education, Ulaanbaatar, Mongolia

[5] Federal Scientific Center of the East Asia Terrestrial Biodiversity Far Eastern Branch of Russian Academy of Sciences, Vladivostok, Russia

[6] Dobretsov Geological Institute of Siberian Branch of Russian Academy of Sciences, st. Sakhyanova 6 «a», 670047, Ulan-Ude, Russia